Ionogel hybrid polymer electrolytes encompassing room-temperature ionic liquids for 4V-class Li-metal batteries operating at ambient temperature

Green Chemistry Letters and Reviews

ISSN: (Print) (Online) Journal homepage: www.tandfonline.com/journals/tgcl20

Ionogel hybrid polymer electrolytes encompassing room-temperature ionic liquids for 4V-class Li-metal batteries operating at ambient temperature

Ying Zhang, Camilla Noè, Giuseppe Antonio Elia & Claudio Gerbaldi

To cite this article: Ying Zhang, Camilla Noè, Giuseppe Antonio Elia & Claudio Gerbaldi (2024) Ionogel hybrid polymer electrolytes encompassing room-temperature ionic liquids for 4V-class Li-metal batteries operating at ambient temperature, Green Chemistry Letters and Reviews, 17:1, 2321247, DOI: 10.1080/17518253.2024.2321247

To link to this article: https://doi.org/10.1080/17518253.2024.2321247

GREEN CHEMISTRY LETTERS AND REVIEWS
2024, VOL. 17, NO. 1, 2321247
https://doi.org/10.1080/17518253.2024.2321247

Ionogel hybrid polymer electrolytes encompassing room-temperature ionic liquids for 4V-class Li-metal batteries operating at ambient temperature

Ying Zhang[a,b], Camilla Noè[c], Giuseppe Antonio Elia [a,b] and Claudio Gerbaldi [a,b]

[a]GAME Lab, Department of Applied Science and Technology (DISAT), Politecnico di Torino, Torino, Italy; [b]National Reference Center for Electrochemical Energy Storage (GISEL) – INSTM, Firenze, Italy; [c]Department of Applied Science and Technology, Politecnico di Torino, Torino, Italy

ABSTRACT

In this study, we prepare ionogels composed of bisphenol A ethoxylate dimethacrylate, poly (ethylene glycol) methyl ether methacrylate, lithium bis(trifluoromethanesulfonyl)imide, and 1-butyl-1-methylpyrrolidinium bis(fluorosulfonyl)imide or 1-ethyl-3-methylimidazolium bis (fluorosulfonyl)imide ionic liquids via rapid, scalable, solvent-free UV-induced polymerization. The various hybrid polymer electrolyte formulations are thoroughly characterized using a comprehensive set of physico-chemical and electrochemical methods, including gel content, FTIR, rheology, DTMA, TGA, SEM, cycling voltammetry, impedance spectroscopy, and galvanostatic cycling in laboratory-scale Li-metal cells. We particularly focus on the influence of using two different ionic liquids as reaction medium on the properties of the resulting materials and their electrochemical behaviors. Our results indicate that viscosity affects the polymerization kinetics of the ionogels, which in turn might affect their thermal stability and galvanostatic cycling behavior. In the purpose of promoting overall performance of solid-state batteries, we also present the results of composite electrolytes obtained by introducing $Li_7La_3Zr_2O_{12}$ (LLZO) into ionogels and following *in-situ* UV-polymerisation. The addition of LLZO ceramic results in more porous solid networks, leading to enhanced charge/discharge stability at ambient temperature and higher C-rates featuring 4V-class NMC cathodes, enlightening the promising prospects of the developed materials to be successfully implemented as stable, durable, and efficient electrolytes in next-generation Li-metal cells.

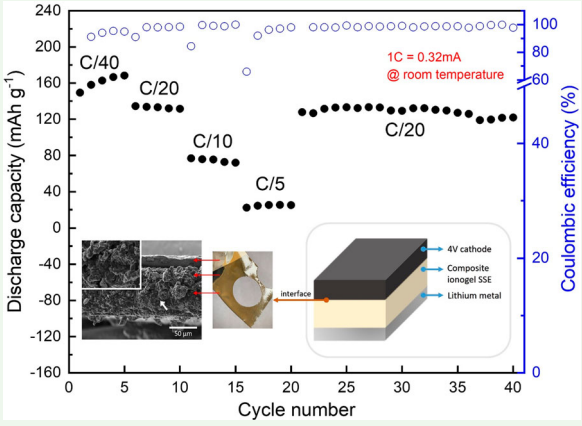

ARTICLE HISTORY
Received 9 November 2023
Accepted 15 February 2024

KEYWORDS
Ionogel; room temperature ionic liquid; polymer electrolyte; composite polymer electrolyte; garnet ion conductor; lithium metal battery

Introduction

The uneven distribution and limits of fossil fuels triggered continuous demand for energy supply is a leading motivation for the development of sustainable and renewable energy storage and conversion systems (*1–3*). Lithium-ion batteries (LIB), which can provide electricity for social energy consumption and be recharged many times, have become, and will in all likelihood continue being, the predominant candidate to power our

CONTACT Claudio Gerbaldi claudio.gerbaldi@polito.it Department of Applied Science and Technology, GAME Lab, Politecnico di Torino, Corso Duca Degli Abruzzi, 24, 10129, Torino, Italy; National Reference Center for Electrochemical Energy Storage (GISEL) – INSTM, Via G. Giusti 9, Firenze 50121, Italy
Supplemental data for this article can be accessed online at https://doi.org/10.1080/17518253.2024.2321247.

portable electronic devices, electric vehicles and much else (*4–7*). Efficient and stable operation of a conventional LIB, comprising an anode, a cathode, and a separator soaked in an aprotic carbonate based electrolyte solution, is significantly impacted by the properties of the electrolyte, emphasizing the need for its suitable formulation selection (*8*). To design a functional electrolyte, it is imperative that certain minimum requirements are met, including being a competent ionic conductor and electronic insulator to promote efficient ion mobility while minimizing self-discharge, possessing a broad electrochemical window to prevent electrolyte degradation within the working potentials of both the cathode and the anode, demonstrating chemical inertness towards the various cell components to prevent unwanted reactions, exhibiting robustness against electrical, mechanical, or thermal adversities, as well as using environmentally friendly and, possibly, low-cost components to promote ecological balance (*9, 10*). However, standard commercial liquid electrolytes are flammable and can pose safety hazards if not handled properly; they can react with the electrodes and generate gas or undergo thermal runaway, which may result in fire or, in worst cases, explosion (*11, 12*).

To address the abovementioned safety issues associated with liquid electrolytes based on organic carbonates, solid-state electrolytes (SSEs) are being investigated as one of the most promising solutions (*13*). In principle, they offer improved safety due to their non-flammable nature, wider electrochemical stability windows, and sufficient ion mobility, which can potentially lead to higher energy densities, longer battery life, and better high-temperature performance (*14, 15*). These advantages make SSEs amongst the best candidates for the development of next-generation batteries that can meet the demands of emerging, high-demanding applications (*16, 17*).

SSEs are generally categorized into solid ceramic (inorganic) electrolytes, solid polymer (organic) electrolytes, and composites thereof. It is crucial to design a SSE characterized by sufficiently high ionic conductivity values, usually in the order of 10^{-4} S cm^{-1} and above, good mechanical integrity and safety, as well as electrochemical and thermal stabilities (*7, 18*). Numerous $Li_7La_3Zr_2O_{12}$ (LLZO) garnet-type solid-state electrolytes (SSEs) have been extensively reported and acknowledged as some of the most promising candidates for deployment in next-generation LIBs, and both experimental and theoretical studies have unveiled the potential to enhance electrochemical capabilities using these electrolyte materials (*19–26*). In the context of Frenkel and Schottky point defects, the movement of Li^+ in LLZO is governed by a combination of vacancy and diffusion mechanisms, where these ions seamlessly diffuse from local sites to adjacent ones, thereby enabling macroscopic-scale ion transport (*17, 27*). Although pure ceramic electrolytes exhibit relatively high Li^+ conductivity/transport, electrochemical and thermal stability, and dendrite suppression capability, their fragility and poor interfacial compatibility with electrodes pose significant drawbacks; in contrast, pure polymer electrolytes offer better interfacial contact and flexibility, but suffer from low ionic conductivity at low temperatures. Proper integration of suitable nonvolatile additives or mixing of the two (or more) inorganic/organic components, resulting in hybrid or composite electrolytes, can overcome these challenges via control of the composition and fabrication processes, allowing for enhanced performance and optimal properties (*16, 17, 28–30*).

One notable approach in the direction of developing SSEs is the integration of room-temperature ionic liquids (RTILs) into a solid matrix, resulting in the creation of a novel hybrid electrolyte system known as an ionogel (or ion gel), which has garnered considerable attention for the application in lithium-based batteries from the 2000s (*31, 32*). RTILs are organic salts with liquid-like behavior at or near room temperature, which are reported to have unique properties to make them highly attractive as electrolytes or reaction solvent/media (*33–37*). Entrapment of RTILs into a solid host material leads to the formation of ionogels, which possess exceptional characteristics that make them appealing for the use as advanced electrolytes, including but not limited to enhanced mechanical strength, higher thermal stability, and superior ion conduction properties (*35, 38–44*).

While the overwhelming majority of current ionogel innovations are focusing on achieving electrolyte systems by combining different polymer hosts with various liquid ion-conducting media and emphasizing their electrochemical performance tests, there has been important research devoted to investigating the effect of the polymerization processing and kinetics on the physical and electrochemical properties. Nair et al. studied polymerization kinetics of UV-cured methacrylic monomers and reported that the inclusion of monomethacrylate as reactive diluent was pivotal, as indicated by membrane tests for ionic conductivity, stability, and cyclability in lab-scale cells (*45*). Porthault et al. found that photocuring sequence, especially the radiation intensity, influences polymer chain length and cross-linking density, leading to different ionic conductivities and mechanical properties (*46*). Susan et al. investigated the solubility of a large number of vinyl monomers in ionic liquids, together with the characterization and

ion transport behavior of ionogels to achieve the goal of molecular design of highly conductive polymer electrolytes (*47*). Andrzejewska and coworkers reported developments in photopolymerization processes carried out in ionic liquids, as well as the photopolymerization of ionic liquid monomers (*34*). Kubisa et al. highlighted the importance and how the kinetics of radical polymerization conducted in ionic liquids might be affected by those media coupled with high viscosity compared to typical organic solvents (*48*).

In previous research works, we studied the electrochemical behavior of different methacrylic-based (solid, quasi solid, and gel) polymer electrolytes, (*49, 50*) consisting of methacrylate-terminated polymers with or without the addition of organic solvents and/or ionic liquids (*45, 51–54*). In the context of ionogel development, understanding polymerization kinetics is essential because it greatly determines the structure, morphology, and properties of the resulting material, which consequently affect the ion transport, the ionic interactions, etc. (*55*). Therefore, in this work, we prepared methacrylic-based ionogels encompassing two common RTILs and carried out a combination of various characterization techniques in order to provide a potential contribution to the development of novel ionogels with desired properties for use in LIBs. Lithium bis(trifluoromethanesulfonyl)imide (LiTFSI) was used in the system as the ion carrier due to its good solubility, wide electrochemical stability window, and high thermal stability (*32*). The cations of RTILs are pyrrolidinium and imidazolium, which are well known for having been used for a variety of investigations (*36, 37, 56*). The FSI anion was chosen to balance some of the electrolyte performances by achieving a potential synergetic effect through mixing with TFSI anion of the salt (*57–59*). Bisphenol A ethoxylate dimethacrylate, a UV-curable difunctional oligomer, was chosen due to its ability to readily form flexible 3D networks by light induced crosslinking. It has been widely used as a crosslinker in the synthesis of hydrogels due to its biocompatibility, low toxicity and viscosity, and commercial availability (*60, 61*). In addition, it was proven that its phenyl rings could contribute to enhanced stiffness of the polymer network (*62*). On the other hand, the monofunctional monomer, poly(ethylene glycol) methyl ether methacrylate, plays a role in the system to reduce T_g and to increase lithium ion mobility due to the presence of ethoxy groups (*45*). The cross-linking polymerization process occurs through a free-radical mechanism in the presence of a methylpropiophenone derivative photoinitiator, and it is composed of three main steps: initiation, propagation, and termination. The photoinitiated cross-linking method shows competitive advantages, such as solvent-free process, good polymerization control, rapid curing, negligible thermal budget, and so forth, which increased industrial interest in its economic and environmental applications (*46, 63, 64*).

Moreover, as hybrid organic–inorganic frameworks for ionogel electrolytes have gained increasing interest among researchers in recent years, (*40*) a preliminary study on two types of composite ionogels was covered in this article, the results of which are presented in the last sessions also compared with the organic ionogel systems. It is suggested that LLZO posseses good resistance towards reduction with Li metal, indicating superior stability compared to other solid electrolytes like LATP, LLTO, LGPS, and LPS; furthermore, between LLZO tetragonal and cubic phases, the cubic phase provides more sites for Li ion migration than the tetragonal phase (*21, 22*). Thus, in this study, the cubic LLZO ceramic was selected as the filler for fabricating composites for combining both high ionic mobility and remarkable electrochemical stability for stable Li-metal cell cycling at ambient temperature with 4V-class cathodes (*65–68*).

Materials and samples preparation

Bisphenol A ethoxylate dimethacrylate (BEMA, average Mn: ~1700, EO/phenol: 15), poly(ethylene glycol) methyl ether methacrylate (PEGMEMA, average Mn: ~500), and 2-hydroxy-2-methylpropiophenone (Darocur1173) were purchased from Merck – Italy. 1-butyl-1-methylpyrrolidinium bis(fluorosulfonyl)imide ($PYR_{14}FSI$), 1-ethyl-3-methylimidazolium bis(fluorosulfonyl)imide (EMIFSI), and lithium bis(trifluoromethanesulfonyl)imide (LiTFSI, battery grade) were purchased from Solvionic.

Scheme 1 shows the chemical structures of the different electrolyte components. Lithium lanthanum zirconate ($Li_7La_3Zr_2O_{12}$, LLZO) was received from Schott and was further sieved to obtain particle size <32 µm. LiTFSI was dried at 150 °C for 24 h before use.

The ionogel electrolytes are composed of a mixture of BEMA and PEGMEMA (70:30 wt%) as the polymer matrix, PYR-based or EMI-based RTIL as the plasticizing ionic mobility enhancer, and LiTFSI as Li^+ source in a ratio of 25.5:59.5:15.0 in weight (see Table 1). After the above-mentioned chemicals were sequentially added together and the salt was fully dissolved by a magnetic stirrer at ambient laboratory temperature in an Argon-filled dry glovebox (MBraun Labstar, O_2 and H_2O content <1 ppm), 5 wt% of photoinitiator (PI, phr) – with respect to the whole weight of each formulation – was mixed into the solution to allow the precursor mixture to be UV-curable. The concentration of the photoinitiator

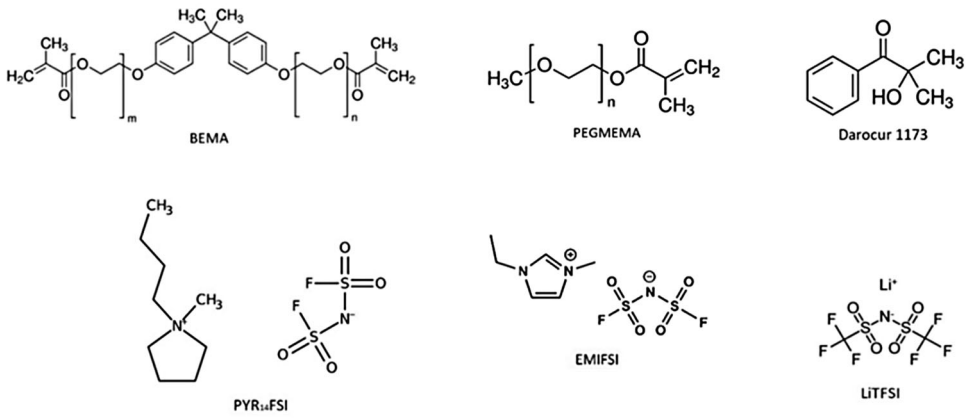

Scheme 1. Chemical structure of BEMA and PEGMEMA oligomers, Darocur1173 photoinitiator, $PYR_{14}FSI$ and EMIFSI room temperature ionic liquids, and LiTFSI salt.

was determined according to the findings of real-time FTIR analysis, which will be discussed later in this paper. Then, the viscous liquid-like precursors were crosslinked into the form of self-standing, ready-to-use membranes by fast 3 min UV-curing, under Ar atmosphere, at 40 mW cm^{-2} by a Helios Quartz medium-pressure Hg lamp. The same method was used to fabricate the composite polymer electrolyte membranes by combining 50 wt% of the aforementioned ionogel precursor system and 50 wt% of LLZO ceramic particles, of which the results will be detailed in the last session of this paper. The use of the 50% in weight of LLZO has been selected as a compromise between maximizing the ceramic content of solid components in the electrolyte and the ability to produce self-standing and mechanically stable membranes. Table 1 shows the detailed proportion of each component, as well as other parameters of the formulations.

Physicochemical and morphological characterization

Real-Time Fourier transform infrared (FTIR) spectroscopy can be used to monitor reaction yields during UV-induced polymerization (UV curing). Formulations were cast on a silicon wafer (film thickness of 12 µm), and the spectra were recorded with a Nicolet iS50 spectrometer before the irradiation, as well as after being UV-cured for 10s, 20s, 30s, 60s, 120s, and 180s time, in both air and nitrogen atmospheres. These tests were carried out on the mixtures prepared with the addition of various amounts of photoinitiator Darocur1173, starting from 1 wt%, and up to 6 wt% where the degree of C = C conversion did not show dramatic improvement. The UV source used was a Fusion System lamp, at an irradiation of 66.7 mW cm^{-2}. The reference 1700–1750 cm^{-1} region can be attributed to the C = O stretching vibrations, while the peak at 1635–1640 cm^{-1} is assigned to the C = C functional group of methacrylates. The calculation was done following Equation (1), where $A_{c=c}$ and $A'_{c=c}$ refer to the areas of the methacrylic C = C peak before and after the photo-curing, respectively, while $A_{c=o}$ and $A'_{c=o}$ refer to the areas of the carbonyl group before and after the photo-curing, respectively.

$$\text{Degree of conversion } (DC,\ \%) = \left(1 - \frac{\frac{A'C=C}{AC=C}}{\frac{A'C=O}{AC=O}}\right) \times 100\% \quad (1)$$

The Thermo Scientific OMNIC Specta Software was used to record and process the data; all measurements were repeated in triplicates and the average values were used to be plotted.

Table 1. Formulations of the ionogels and composite ionogels under study.

Formulation Names	Polymer matrix	Ionic liquid (RTIL)		Li salt	Ceramic				
	BEMA/PEGMEMA (70/30)	$[PYR_{14}][FSI]$	[EMI][FSI]	LiTFSI	LLZO		EO/Li	Li/IL	Density (g/mL)
PYR-ionogel	25.50 wt%	59.50 wt%	–	15.00 wt%	–		8.70	0.28	1.328
EMI-ionogel	25.50 wt%	–	59.50 wt%	15.00 wt%	–		8.70	0.26	1.424
PYR-composite	12.75 wt%	29.75 wt%	–	7.50 wt%	50 wt%	20.65 vol%	8.70	0.28	–
EMI-composite	12.75 wt%	–	29.75 wt%	7.50 wt%	50 wt%	21.82 vol%	8.70	0.26	–

Note: 5.1 g cm^{-3} was used as the density of LLZO (*69*) for calculating the ceramic volume. Values of EO/Li and Li/IL are in molar ratio. The density of ionogels was measured by mass/volume ratio.

Rheological measurements were conducted to evaluate the viscoelastic properties of the materials, including shear, time, amplitude, and frequency sweep tests using a rheometer (Physica MCR 302, Anton Paar, Graz, AUT) in parallel plate mode with a fixed gap of 0.3 mm. The viscosity of the samples was recorded by varying the shear rate (γ) from the lowest value to the highest value (γ = 0.01–100 s^{-1}, respectively). Photorheological tests were conducted using a UV-light source (Hamamatsu LC8 lamp, Hamamatsu Photonics, Shizuoka, JPN) with a light intensity of 28 mW cm^{-2} placed under a quartz plate with the formulation to monitor the gel formation by following the evolution of storage modulus with time. The UV light was turned on after 30 s of equilibration time before the onset of polymerization. Time sweep measurements were performed during irradiation at a constant frequency of 1 Hz within the linear viscoelastic region (strain amplitude γ of 1%), based on preliminary amplitude sweep tests.

The crosslinked fraction (gel content) was evaluated to study the crosslinking density, determined by extracting the soluble components in acetonitrile. Both before and after the extraction, the samples were dried under vacuum at 70 °C overnight and then placed in the glovebox for being weighed when their constant weight values were obtained. The insoluble fraction mass was calculated based on the following equation (Eq 2):

$$\text{Gel content} = \frac{\text{Insoluble fraction weight}}{\text{Initial sample weight} \times \text{Polymer proportion}} \quad (2)$$

The crosslinked membranes achieved from photorheology measurements were subjected to thermogravimetric analysis (TGA). Each sample was tested by TG 209 F3 Tarsus Thermogravimetric Analyzer (NETZSCH-Gerätebau GmbH) in the alumina crucible under a N_2 flow with a heating rate of 10 °C min^{-1} up to 700 °C.

Dynamic thermal-mechanical analysis (DTMA) was performed with a Triton Technology to evaluate the dynamic mechanical properties of electrolyte membranes by applying uniaxial stretching to the sample with a heating rate of 3 °C min^{-1}, starting from −100 °C, and at a frequency of 1 Hz and strain of 0.02%. The approximate sample dimension used in the test was 11 mm x 7 mm x 0.5 mm (length × width × thickness). The storage modulus (E′), loss modulus (E″) and damping factor (tanδ) were recorded as a function of the temperature. The glass transition temperature (T_g) was assigned at the maximum damping factor (tanδ = E″/E′).

The surface morphology of the polymer-based electrolytes was studied by field emission scanning electron microscopy (FESEM). For obtaining the cross-sections for analysis, a dipping process in liquid nitrogen was implemented to crack the samples while properly preserving their morphology. SEM images were subsequently captured using a ZEISS Supra 40VP instrument, operating at an accelerating voltage of 5 kV, to obtain high-quality micrographs for accurate analysis.

Electrochemical measurements

ECC-Std (EL-CELL, Germany) lab-scale test cells were used for all the electrochemical tests; all cells were assembled under the controlled atmosphere of an Ar-filled dry glove box (MBraun UniLab, H_2O and O_2 < 1 ppm). For specified operating temperatures, a climatic chamber (Binder MK53 E2) was used to accurately control the operational temperature of the cells.

For ionic conductivity tests, each electrolyte membrane sample, being placed between two identical stainless-steel (SS-316) electrodes, was excited at the open circuit potential (OCV) by a small amplitude AC sinusoidal potential of 20 mV in the frequency range between 300 kHz and 1 Hz, and the corresponding impedance was recorded through a VMP-3 electrochemical workstation from BioLogic Science Instruments (France). Cells assembled with ionogel electrolyte formulations of PYR-ionogel and EMI-ionogel were tested at different temperatures, starting from −20 °C and up to 80 °C (10 °C temperature step). The ionic conductivity was calculated by equation (3): where R_b is the bulk resistance, and *A* and *l* refer to the area and thickness of the electrolyte sample, respectively:

$$\sigma = \frac{l}{A \cdot R_b} \quad (3)$$

The electrochemical stability window (ESW) plays a fundamental role in determining the durability and energy output of a Li-based cell. ESW of the ionogel electrolytes was evaluated by linear sweep voltammetry (LSV) of a Li/ionogel/Al(carbon-coated) cell configuration in the voltage range of 2.7−5.3 V vs Li^+/Li for determining the anodic stability window (ASW), and a Li/ionogel/Cu cell in the voltage range from −0.5 to 3 V vs Li^+/Li for estimating the cathodic stability window (CSW). The measurements were carried out at ambient temperature by the Biologic VMP-3 potentiostat.

To study the interfacial properties of the UV-cured ionogels against the lithium metal electrode, electrochemical impedance spectroscopy (EIS) experiments were carried out through the Li-Li symmetrical cell configuration, in which a sample of ionogel membrane was sandwiched between two identical lithium metal electrodes. The cells were stored at ambient temperature at the OCV and connected to the VMP-3 potentiostat, and the variation of the resistance as a function of contact time was measured.

Li/ionogel membrane/Li symmetric cells were assembled and used for long-term lithium stripping/plating tests at ambient temperature from OCV by the VMP-3 potentiostat. During each cycle, both Li-plating and Li-stripping were carried out for 3 h (each) at current densities of 25 μA cm^{-2}, which is approximately equivalent to C/25 current rate used for ionogel sample cycling in this study (see below). Lithium electrode surfaces were cleaned with a brush and smoothed using a clean and dry polypropylene sheet before use.

The lab-scale Li-metal cells were assembled with a $LiNi_{0.5}Mn_{0.3}Co_{0.2}O_2$ (NMC-532, BASF) cathode, an ionogel polymer or composite ionogel electrolyte membrane and galvanostatically cycled against Li metal as the counter electrode. The cathode consisted of 85 wt% NMC-532 active material, 10 wt% carbon black (Denka) conductivity enhancer, and 5 wt% polyvinylidene difluoride (PVdF, Solvay Solef 6010) binder blended in N-methyl-2-pyrrolidone (NMP, Sigma-Aldrich); it was prepared by the slurry-casting-drying method without calendering. Rather low (< 2 mg cm^{-2}) mass loading was used to achieve better interfacial contact of the solid-state electrolyte samples with the porous cathode (*70*). In addition, the electrolyte precursors were also cast (by a doctor blade) and photocured onto the surface of the dried cathodes to enhance electrolyte percolation through the bulk of the electrode, thus achieving optimal active material utilization. After 15-20 min vacuuming in the glovebox chamber (under 1 Pa), the same photocuring procedure detailed previously was conducted. The resulting, ready-to-use electrodes conformally coated with the ionogel polymer electrolyte were directly assembled in the test cells and equilibrated at ambient temperature for 72 h before testing. Cell cycling was performed in terms of constant current (galvanostatic) discharge/charge steps at different current rates using an Arbin BT-2000 battery tester between 3.0 and 4.3 V versus Li^+/Li at ambient laboratory temperature of around 21 °C. The applied current regimes were calculated based on the mass loading of each used NMC-532 cathode, which is proportional to the product of the theoretical capacity of NMC-532 material (185 mAh g^{-1} in practice) and NMC-532 active material mass in the cathode.

Results and discussion

Materials characterization

The first set of analyzes examined the impact of different photoinitiator (PI) concentrations on the C=C conversion degree of ionogel samples (namely, PYR-ionogel and EMI-ionogel). The photo-initiator was a benzoin ether derivative, which generates radicals by an intramolecular scission, leading to the conversion of the double bonds of the dimethacrylate BEMA, the propagation of which leads to the formation of a rather flexible three-dimensional network; the addition of the mono-methacrylate reactive diluent, which is incorporated into the network, modifies the polymeric membrane properties, tailoring them as desired, (*49*) and it is expected mainly to reduce the T_g of the macromolecular network and to increase the mobility of lithium ions in the polymer matrix by the presence of ethoxy groups (*53*). The crosslinking of UV-curable ionogels can be monitored accurately using FTIR, and the spectra, both before and after UV-curing, for samples containing 5 wt% of photoinitiator are shown in Figure S1 within the supplementary information. Figure 1 displays a similar trend of increasing degree of conversion (DC) of two systems with increasing amount of added photo-initiator; the reactivity of all the monomers is very high in the initial stages of the UV-curing and reaches its maximum very rapidly. However, it is interesting that the DC was observed to be lower with 6 wt% of PI than that with 5 wt% PI in PYR-based formulation. This phenomenon could be due to the radicals quenching: the reactions of primary radicals would compete with the double bond during the initiation. Furthermore, with increasing PI concentration, the DC trend in the medium of EMIFSI ionic liquid showed a continuous increase and higher efficiency compared to samples of PYR-ionogel, which might originate from lower viscosity of imidazolium-based RTIL that promotes better flow of the mixture, and perhaps also caused by the relatively higher polarity of its cation that leads to better solvation ability or mixability with the monomers (*34*).

Scheme 2 demonstrated the preparation of the SSE membranes used in this study and the polymer matrix structure after UV-polymerization process. The obtained self-standing, transparent, homogeneous, and flexible crosslinked ionogel membranes with 5 wt% of PI, shown in Figure 2(A), implied good processing feasibility. The 5 wt% of PI demonstrated the optimal balance between C=C conversion degree and the objective of minimizing additional components in the battery electrolyte systems. It is important to note that the ATR-FTIR spectra of the cured samples only provide qualitative information, as the technique does not allow for quantitative analysis of the degree of cross-linking or the amount of residual functional groups in the polymer network (*71*, *72*). As a result, the efficiency of the curing process was assessed by determining the gel or insoluble fraction content after extraction in acetonitrile. The gel content was calculated to be 88.80

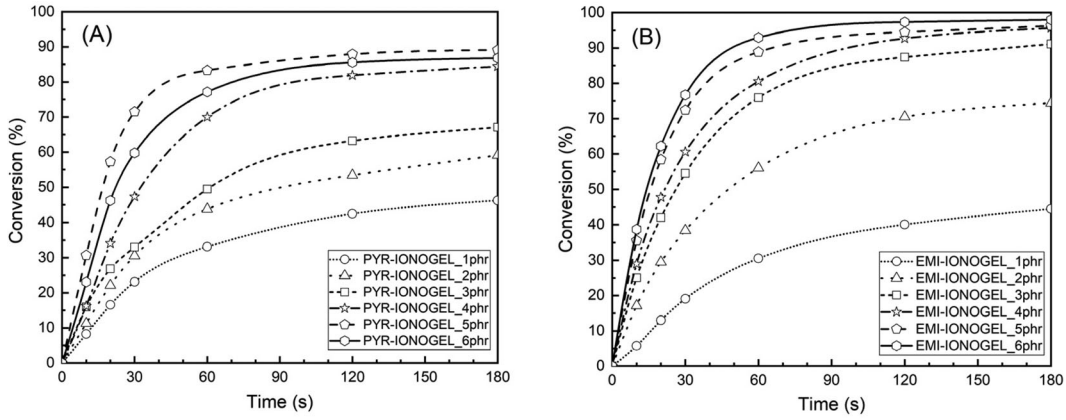

Figure 1. Conversion of (A) PYR-based and (B) EMI-based ionogel systems versus exposure time for different photoinitiator (phr) concentrations, ranging from 1 to 6 wt% (1phr – 6phr), at room temperature.

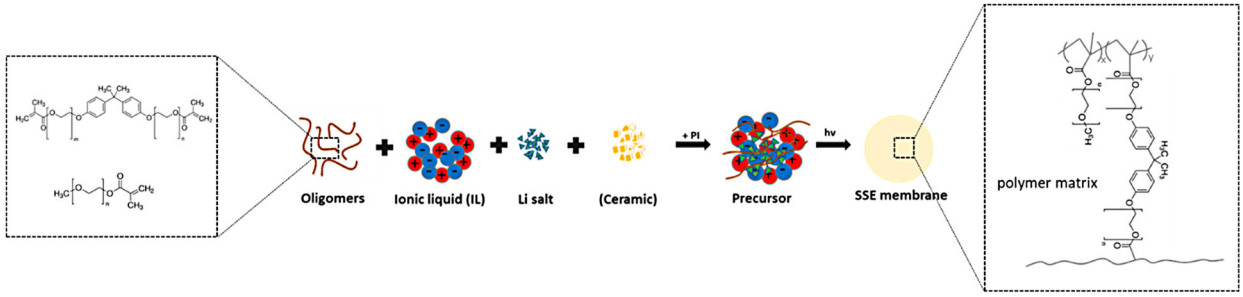

Scheme 2. Preparation of SSE membranes in this study and polymer matrix structure after UV-polymerization.

and 96.85% for PYR-based and EMI-based ionogels, respectively. The high values obtained for the two experimental groups would suggest that the UV-curable systems have undergone efficient conversion, resulting in highly cross-linked polymer networks that are expected to have high mechanical strength and good thermal stability without leakage of the encompassed ionic liquid fraction (*13*). Figure 2(B) shows composite electrolyte membranes UV-crosslinked after photorheology measurements. Notably, the membrane exhibited excellent flexibility as it was able to withstand multiple folding and releasing cycles without any breaks (Figure 2(C,D)), indicating their promising flexibility and overall mechanical robustness, which are important characteristics for a SSE. For the composite electrolyte, the PI 5% mass ratio corresponds to the entire mass of each composite-based electrolyte precursor, thus leading to a PI of 10% mass with respect to the ionogel proportion. A higher percentage of PI with respect to the ionogel proportion was selected to avoid potential hindrances to achieving the complete activation of initiating species and the penetration of incident radiation.

Understanding the rheological performance of polymeric materials is of particular importance when dealing with polymerization operations and analyzing

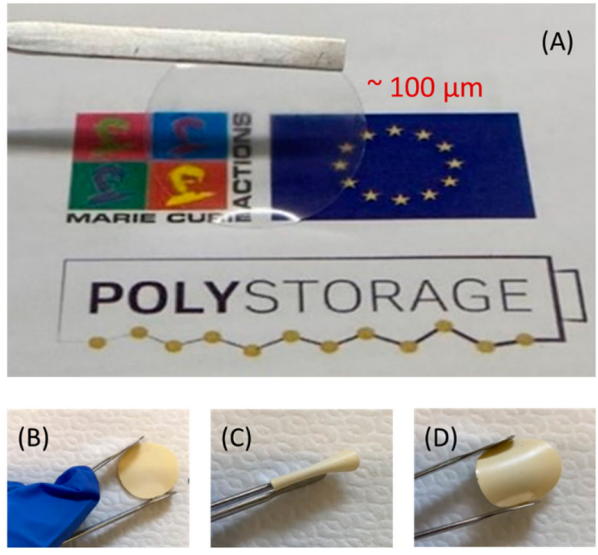

Figure 2. Digital photos showing the UV-polymerised self-standing electrolytes under study: (A) the prepared thin and ready-to-use ionogel solid electrolyte membrane (~100 µm thickness), and the fabricated composite ionogel electrolyte (B). All composite membranes demonstrate good flexibility and mechanical robustness after multiple times being folded (C) and then released (D).

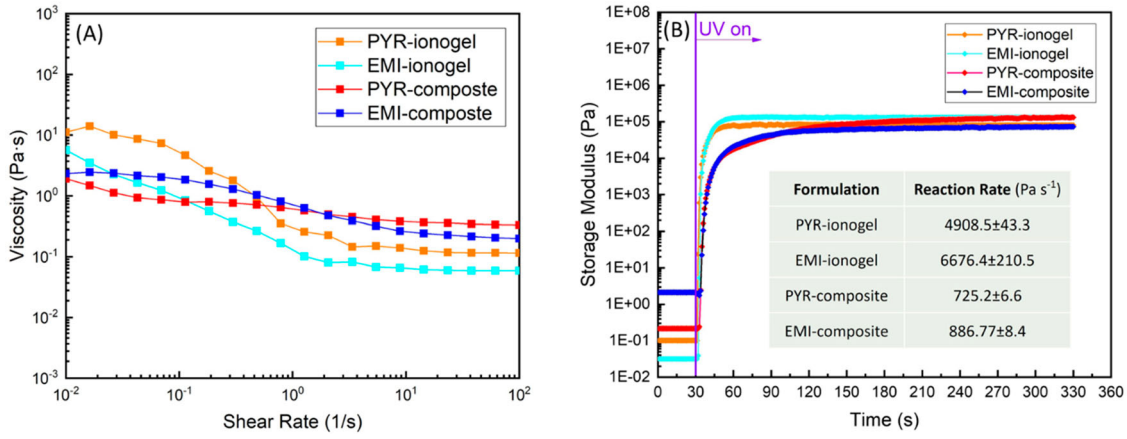

Figure 3. (A) The viscosity of all precursor samples with respect to shear rate, and (B) their storage modulus as a function of UV-curing time and each reaction rate calculated based on corresponding initial slope.

interactions or coordination within systems. According to the results in Figure 3(A), which illustrates the behavior of the resistance to flow of the electrolyte precursors, all samples showed shear thinning properties. Between ionogel systems, as expected, the pyrrolidinium-based pre-polymer electrolyte showed more viscous behavior than the imidazolium-based one. In the case of polymeric composite precursors, the two mixtures exhibited very close values of viscosity at the shear rate of 0.01 s^{-1}, after which EMI-composite showed higher viscosity values, as compared to the PYR-composite system, when the shear rate increased up to around 10 s^{-1} and further. This phenomenon can be associated with a relatively bigger volume of LLZO particles in EMI-composite (as shown in Table 1) that brought higher friction forces (*73*). When the shear rate was big enough, the particle clusters were broken down and dispersed more uniformly throughout the fluid, which caused lower values in viscosity. In addition, the viscosity can be observed to marginally increase in some of the formulations at some points. This behavior is likely ascribed to temporary network structures that still had time to be formed and, thus, temporarily led to an apparent increase in viscosity. It is worth noting that both composite systems exhibited relatively lower solid-like characteristics than ionogels when at initial shear rates, which could be ascribed to the reduced coordination bonds resulting from the destruction of introduced ceramic particles. As the sheer rate increased, the excessive physical bonds in ionogels started being broken down, which led to a neat decrease in the viscosity values (*74*).

The photorheological performance of the four formulations under study, as shown in Figure 3(B), can be demonstrated in the form of several contributions. All the formulations showed very short induction time and reached plateaus after a few minutes, suggesting that the materials are highly responsive to UV-light and suitable for being prepared by photopolymerization. The relatively slower response of composites to the light, as well as their slower polymerization rates that are reflected in the initial slopes of modulus curves, compared to ionogels, imply the presence of inorganic particles that blocked or absorbed a portion of the UV light. Longer curing time was, thus, needed for fully polymerizing composite samples. After 3 min of photo-curing of ionogels and 5 min curing for composites, which are the UV-polymerization time used for obtaining solid electrolytes in this work, we can assume that all the samples are fully crosslinked. Besides, the final storage modulus of PYR-composite surpassed that of PYR-ionogel thanks to the blending of ceramic; surprisingly, the EMI-composite exhibited a relatively lower final modulus value. This unexpected phenomenon is credited to a bit more ceramic volume proportion or/and bigger aggregates occurred in EMI-composite as we mentioned previously about viscosities, and hence the actual UV irradiation to the polymeric components was reduced so that the mechanical properties were influenced (*46*). Further investigation is needed to determine the underlying causes and to further optimize the system as well as the preparation procedure.

The TGA and DTG curves for UV-polymerized PYR-ionogel/composite and EMI-ionogel/composite SSEs are shown in Figure 4(A). Both ionogels started to decompose at above 205 °C and both composites at above 283 °C. The PYR-based ionogel as well as composite systems displayed more bumpy reducing apparent decomposition curves compared to both EMI-based

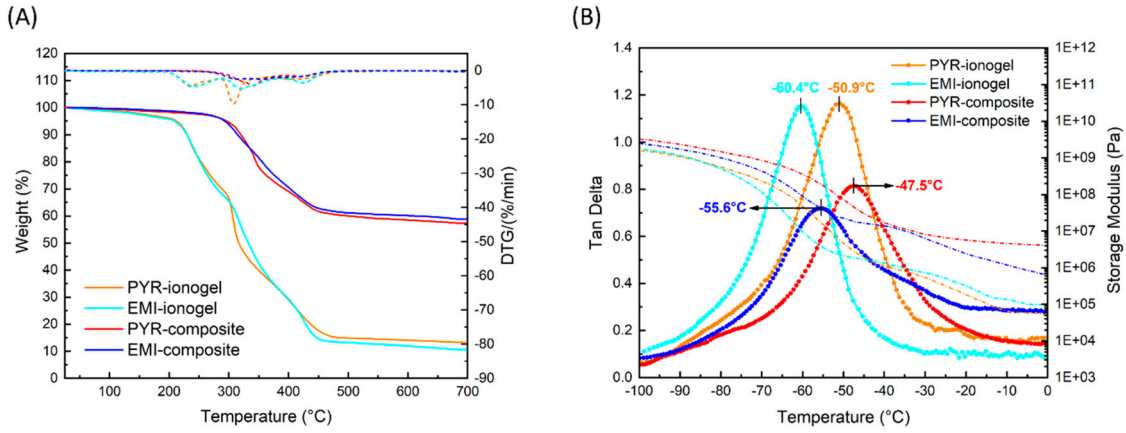

Figure 4. (A) TGA (solid) and DTG (dash) traces and (B) tan δ with storage modulus as a function of temperature of UV-cured samples PYR-ionogel/composite (in orange/red) and EMI-ionogel/composite (in cyan/blue). The glass transition temperatures of all the four formulations are also indicated in (B).

SSEs, which could be potentially explained by their more heterogeneous and uneven curing process influenced by the higher viscosity of $PYR_{14}FSI$ ionic liquid (*74*). Moreover, it is well to be observed that the thermal decomposition rate of samples decreased with the addition of inorganic filler. The ceramic significantly increased the residual weight of the material and slowed down its decomposition rate. These results suggest that the incorporation of filler material significantly impacts the thermal properties and decomposition behavior of solid electrolyte membranes. Furthermore, it is evident from the initial weight loss difference between ionogels and composites that the composites are more resistant to moisture, considering that all sample membranes were stored in the normal air environment in the lab before thermal analyses.

DTMA defines the glass transition in terms of a change in the coefficient of thermal expansion (CTE) as the polymer goes from glass to rubber states with the associated change in free molecular volume. The glass transition temperature (T_g) can also be considered a measure of compatibility or miscibility in polymer blends. As shown in Figure 4(B), a single temperature of glass transition of each sample demonstrates full compatibility between the polymer matrix and RTIL, and the low values suggest a good segmental motion of the polymer chain, which is crucial for ionic conductivity in polymer electrolytes (*42*). Furthermore, the study indicates that the storage modulus of all samples decreased as the temperature increased, providing evidence that elevated temperatures can induce relaxation of the amorphous region through increased chain movement, regardless of the presence of fillers. As expected, adding fillers in the matrix led to an increase in stiffness, as attested by the increase in the storage modulus. It can be observed that the addition of LLZO ceramic resulted in the Tanδ maximum shifting towards higher temperature, indicating efficient stress transfer between the matrix and the inorganic filler and effective reinforcement of the matrix that promoted the thermo-mechanical stability of the samples, as reported by other authors (*71*, *75*). On the other hand, the reinforcement effect, or to say, the presence of the particles that impede the movement of polymer chains by creating ceramic-polymer and ceramic-ceramic interactions might lead to a minor decrease in ionic conductivity values. The Tanδ peak observed in the composites is broader and less pronounced than that of the ionogels, suggesting a more gradual transition; in addition, the shorter heights observed in the composites imply that they have lower elastic properties.

Figure 5 illustrates the surface images obtained through FESEM analysis of the UV-polymerized PYR-composite (A, zoomed image in B) and EMI-composite (C, zoomed image in D). Despite the presence of LLZO aggregates in both composites, the images reveal a well-dispersed distribution of particles throughout the membranes, indicating a favorable interaction. This homogeneous dispersion is crucial for optimizing the interface and highlights the superior performance of these composites compared to traditional ceramic/ceramic interfaces, emphasizing the importance of effective particle dispersion in enhancing overall composite properties.

Electrochemical tests of polymeric ionogel systems

In this study, the ionic conductivity of crosslinked ionogels was investigated. The obtained data are shown in the form of Arrhenius plots (Figure 6). The ionic conductivity behavior versus temperature was calculated

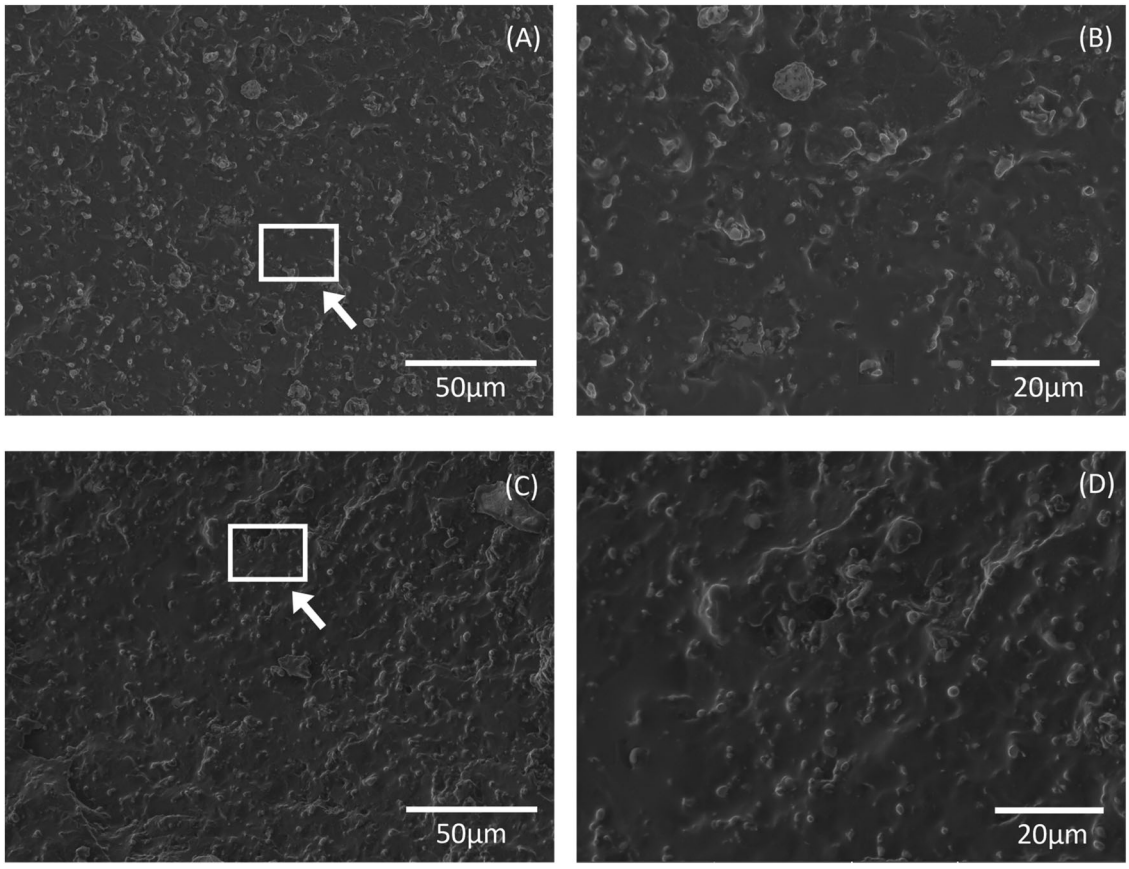

Figure 5. FESEM top view of PYR-composite (A) and its magnified region (B), and FESEM top view of EMI-composite (C) and its magnified region (D). Note that the magnified region in the right handside images correspond to the area indicated by the white square in the left handside images.

according to equation (4), where σ is the ionic conductivity, A is the pre-exponential factor, E_a is the activation energy for the process, R is the gas constant, k is the Boltzmann constant, and T stands for temperature in Kelvin. All the four systems showed high ionic conductivity, especially PYR-ionogel and EMI-ionogel reached values of 0.8 and 1.7 mS cm^{-1} respectively at 20 °C, suggesting they have the potential application in ambient temperature LIBs. In the whole temperature range, the ionic conductivity increases with a linear, VTF-like dependence for all the samples. The composites have lower conductivity values compared to their corresponding ionogel systems, which is likely ascribed to the introduced LLZO ceramic used that also possess slightly lower conduction performance than ionogel formulations. In addition, the EMI-based ionogel/composite have lower activation energy, and exhibited higher ionic conductivity values across the entire temperature range, which can be attributed to the lower viscosity of the EMIFSI ionic liquid.

$$\sigma = \frac{A}{T}\exp\left(-\frac{Ea}{kT}\right) \tag{4}$$

In addition to ionic conductivity, the ionogel samples under study demonstrated reasonably wide electrochemical stability windows (ESW). The current–potential

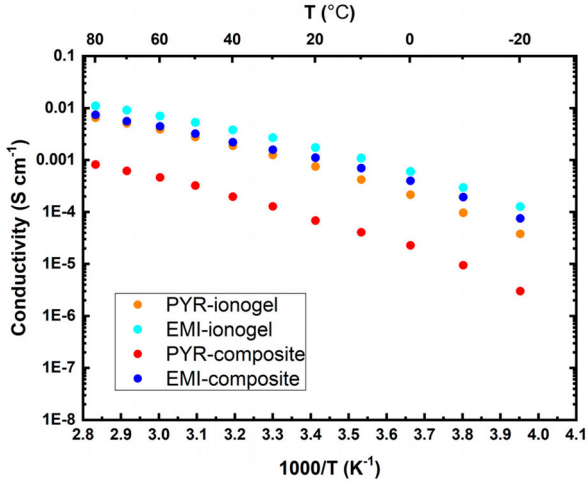

Figure 6. Arrhenius plot showing the ionic conductivity as a function of temperature for PYR-ionogel (in orange), PYR-composite (in red), EMI-ionogel (in cyan), and EMI-composite (in blue) samples.

response measured at ambient temperature by means of linear sweep voltammetry is shown in Figure 7. PYR-ionogel performed better reduction stability than EMI-ionogel, which is related to the reactive hydrogen atom on C-2 position of the imidazolium cation (*37*).

ESW was assessed using a slow scan rate (0.1 mV s^{-1}) to allow the detection of any oxidation process (*70*). A small current flow can be observed just above 4 V, ascribed to the formation of side-/by-products, whereas the anodic breakdown occurs at about 4.6 V vs Li^+/Li. The attainment of an electrolyte with a notably wider anodic stability would mark a significant achievement, particularly with regard to its potential use in battery cells featuring 4V-class cathodes, such as $Li(Ni_{0.8}Co_{0.15}Al_{0.05})O_2$ (NCA), $Li(Ni_xCo_xMn_x)O_2$ (NMC), $LiCoO_2$ (LCO), and so on (*76*, *77*).

Electrochemical impedance spectroscopy (EIS) assisted us with characterizing the resistances that develop at the interfaces of the lithium-metal symmetric cells in electrolytes of PYR-ionogel (Figure 8(A)) and EMI-ionogel (Figure 8(B)). The relevant change at low frequency is also shown in Figure S2 in the supporting information. The interfacial resistance in both ionogel systems experienced a slight fluctuation during the first few days, but showed an overall downward trend, suggesting a reorganization process of the passivation layer, which led to a more uniform, compact, and less resistive structure at the interface over time. After around 5 days, time-stable resistance was achieved. The behavior observed is closely related to the initial formation and stabilization of the Solid Electrolyte Interphase (SEI) layer and the subsequent improvement of contact over time at the interface between the lithium metal electrode and the polymer electrolyte, which is typical of the majority of polymer electrolytes (*78*). Moreover, PYR-ionogel demonstrated a faster and more stable interfacial layer towards lithium, which is in agreement with the reduction stability window results and is related to the nature of different cations in RTILs (*33*, *37*).

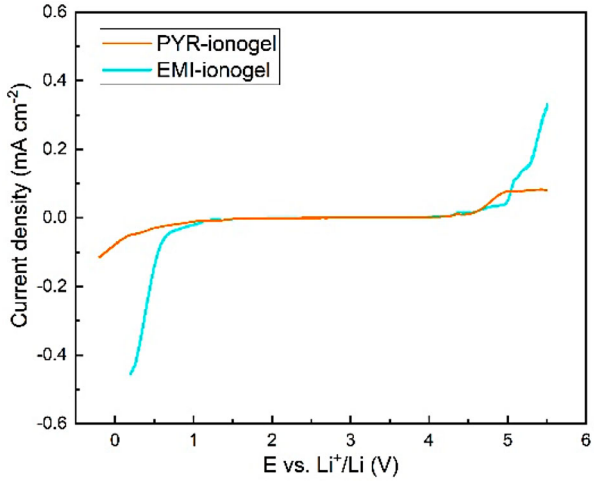

Figure 7. Electrochemical stability windows of sample PYR-ionogel (in orange) and EMI-ionogel (in cyan). The anodic and cathodic scans were separately collected at room temperature and then combined.

Lithium plating/stripping measurements were performed in Li/ionogel/Li symmetric cells to determine the lifetime of solid-state batteries by monitoring lithium dendrite nucleation and growth resistance (*78*). Long-term cycling results (600 h, 100 cycles) of PYR-ionogel and EMI-ionogel at 25 μA cm^{-2} current density (electrode area: 2.011 cm^2) with both the plating or the stripping steps lasting for 3 h each are shown in Figure 9. Low overpotentials were obtained (in the range of 0.055 V upon initial cycling, which increased only slightly up to 0.075 V at the end of the test) without any short circuit occurred. This test assures the effectiveness and safe operation of the ionogels in lithium-based cells conceived for ambient temperature applications. Despite the low current density used in the process, it can be inferred that this is a promising path to pursue for future studies, given the good indication of its potential for solid-state electrolyte systems operating at standard ambient conditions.

To demonstrate the practical application of ionogels, galvanostatic cycling was conducted on lab-scale cells assembled with ionogel-in-situ-polymerized-on-NMC electrodes and lithium metal at ambient temperature, where the direct crosslinking step was fundamental to achieve a good electrode/electrolyte interfacial adhesion, resulting in a stable and thin (approximately 30 μm) ionogel electrolyte film with uniform distribution over the electrode (*79*, *80*). Figure 10(A) shows cross-sectional secondary electron FESEM images of PYR-ionogel (representative for all the samples prepared) that clearly revealed an intimate and compatible interface between the cross-linked polymer matrix and the NMC cathode, which also indicates that the ionogel is highly cross-linked, as evidenced by its bulky structure. Additionally, in Figure 10(B), the *in-situ* polymerized composite also exhibits intimate contact with the cathode. A porous structure is observed, suggesting that the composite has potentially favorable morphology for efficient ionic transport by providing appropriate room for hosting ILs. Furthermore, the image confirms the effective dispersion of LLZO particles throughout the electrolyte. The image evidences the very intimate interconnection between the electrode film and the electrolyte, with a very good interpenetration of the electrolyte components in the electrode porosity; in fact, from the image, it is not possible to recognize a separation between the electrolyte film and the electrode. The

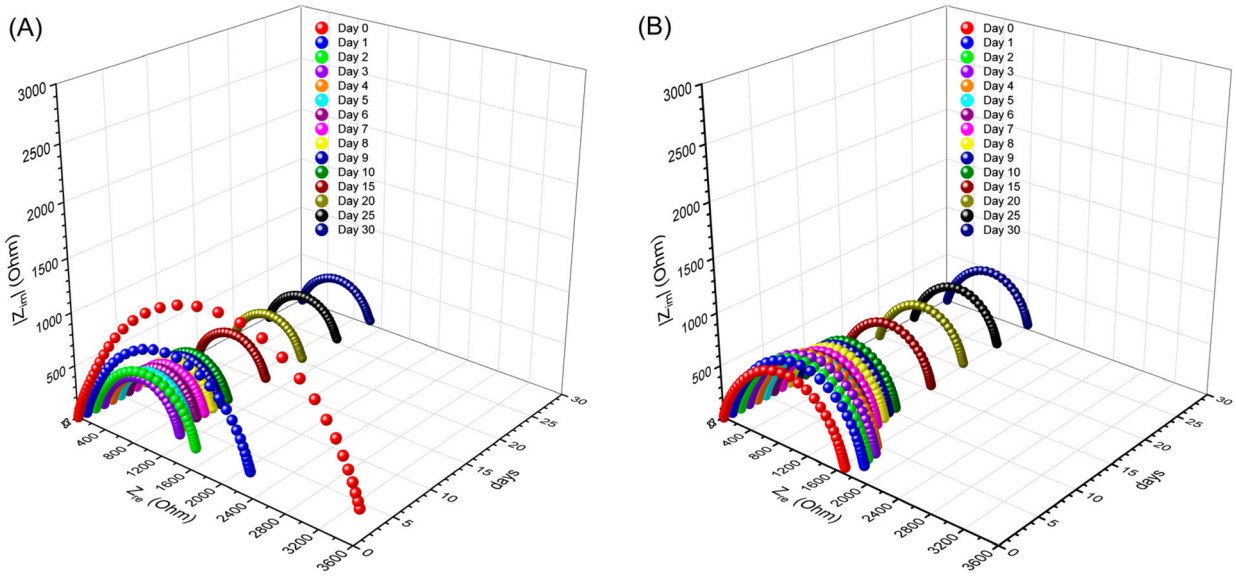

Figure 8. 3D Nyquist plots representing the evolution of the interfacial resistance over time for samples of (A) PYR-ionogel and (B) EMI-ionogel, by using Li/ionogel/Li cells configuration, stored under O.C.V. conditions at a constant temperature of 25 °C. Electrode area: 2.011 cm^2. Frequency range: 1 Hz – 100 KHz.

measurement evidences that the overall thickness of the electrode and membrane is about 30 µm for the ionogel and 60 µm for the composite. Overall, *in-situ* polymerization illustrated good contact between electrolyte and cathode, which is crucial for achieving high room-temperature ionic conductivity and fast interfacial charge transport for practical operation of solid-state batteries (*81*, *82*).

Figure 11(A–D) show the constant current charge/discharge specific capacities vs. cycle number and voltage profiles of PYR-ionogel and EMI-ionogel samples, respectively, which were collected at ambient laboratory temperature (~21 °C) and at different C-rates from C/40 to C/10. The charge/discharge profiles for PYR-ionogel (Figure 11(A)) and EMI-ionogel (Figure 11(C)) electrolytes are observed to be tilted rather than a flat line, which can be attributed to their intrinsic low ionic conductivity at room temperature when compared to that of organic carbonate electrolytes and/or pure ionic liquid electrolytes (*83*). The results in terms of delivered specific capacity suggest that the ion diffusion is the limiting factor to achieve high power output in our ionogel-based solid polymer cells (maximum achieved C-rate of C/10), as confirmed also by EIS measurements, as well as by the increasing overpotential at higher C-rates. Nevertheless, the PYR-ionogel cell exhibited an initial discharge capacity of 182 mAh g^{-1}, while the EMI-ionogel cell exhibited a slightly lower initial discharge capacity of 171 mAh g^{-1} at C/40. The lower capacity of the EMI-ionogel cell may be attributed to its higher applied currents (e.g. 1C = 0.65 mA, compared to 1C = 0.51 mA for PYR-ionogel) that were determined based

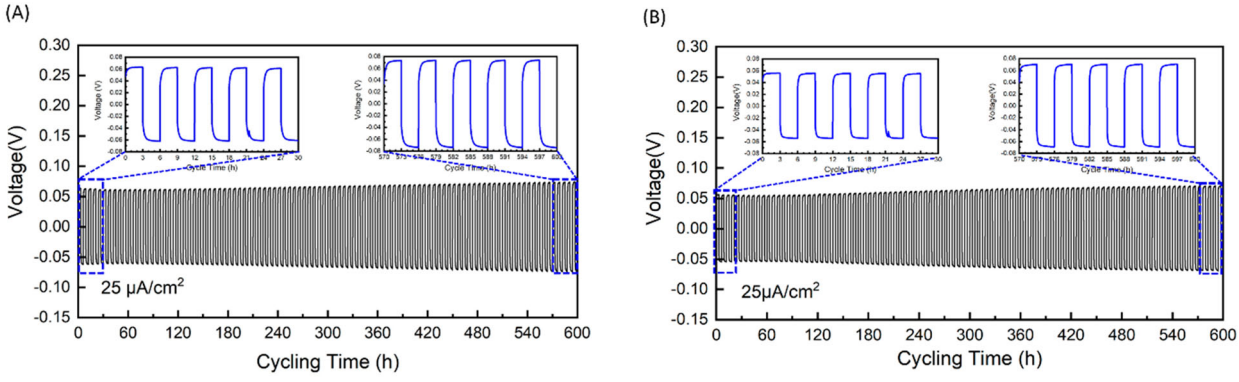

Figure 9. Stripping/plating voltage profiles of the Li cycled with the (A) PYR-ionogel and (B) EMI-ionogel electrolyte membranes at 25 µA cm^{-2} at ambient laboratory temperature as well as their local view of voltage profiles.

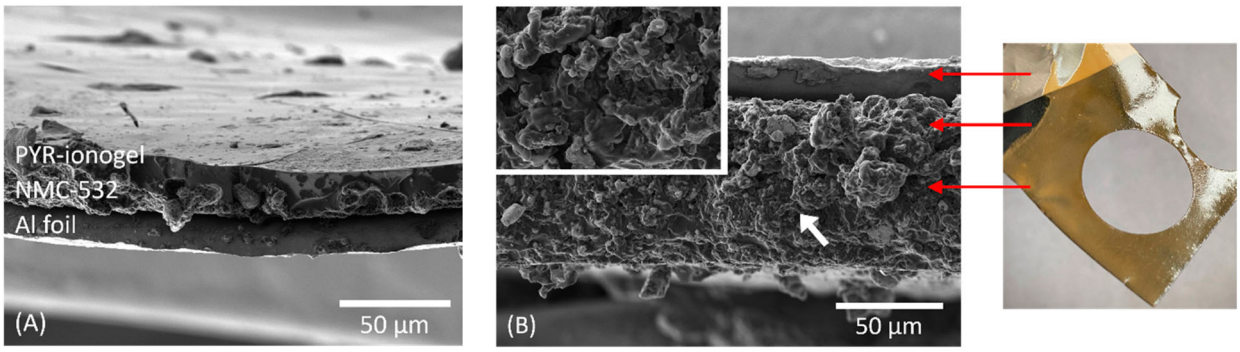

Figure 10. FESEM cross-sectional images of (A) PYR-ionogel and (B) PYR-composite, *in-situ* UV-polymerized on NMC-532 cathodes.

on actual cathode mass loadings. As shown in Figure 11 (B,D), gradual capacity fading occurred during charge/discharge, which was more pronounced for the PYR-ionogel cells at increased C-rates. This phenomenon might be linked to the presence of unreacted residual monomers in the ionogels after *in-situ* polymerization, which tend to decompose or deposit on the surface of the electrodes, and, thus, increase the electrode//

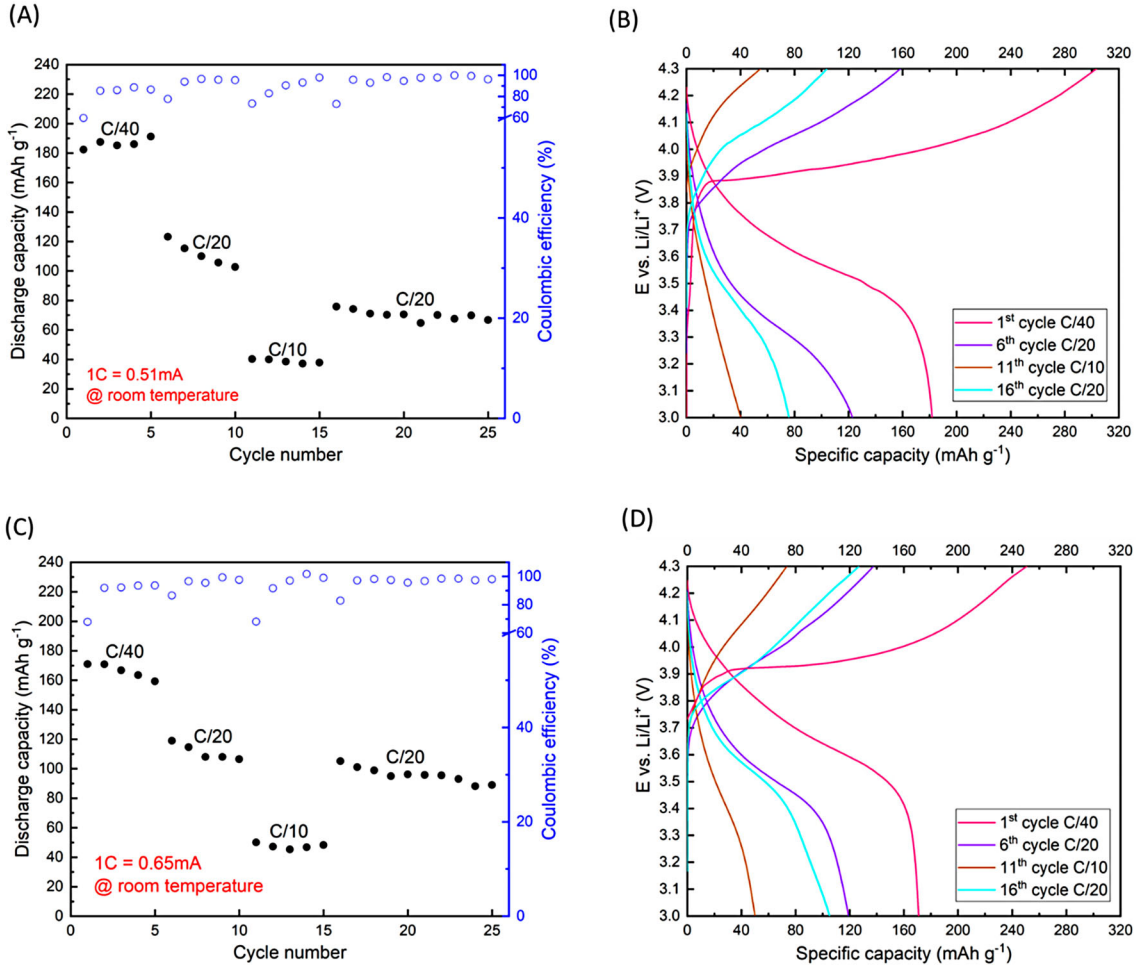

Figure 11. Ambient laboratory temperature (~21 °C) galvanostatic cycling behavior of the lab-scale cells with ionogel electrolytes at different current densities: (A) specific discharge capacity and Coulombic efficiency vs. cycle number and (B) discharge/charge potential vs. specific capacity profiles of PYR-ionogel cell (1C = 0.51 mA, calculated based on the active material mass loading of 1.77 mg cm^{-2}); (C) specific discharge capacity and Coulombic efficiency vs. cycle number and (D) discharge/charge potential vs. specific capacity profiles of the EMI-ionogel cell (1C = 0.65 mA, calculated based on the active material mass loading of 1.74 mg cm^{-2}).

electrolyte interfacial resistance, resulting in a deterioration of cycle performance, especially at low temperatures or high rates (*13*). According to the characterization results of the polymers in the two ionogel formulations discussed earlier, it was found that the EMI-ionogel exhibited a more uniform and higher degree of crosslinking/polymerization. This may explain why the cell with EMI-ionogel exhibited less capacity fading in its galvanostatic cycling profile, as the higher degree and homogeneity of crosslinking/polymerization structure could have contributed to a reduction in the content of residual monomers and an increase in uniformity. Such improvements in the polymer structure have been already potentially shown to enhance the electrochemical performance of polymer-based batteries (*13*).

Overall, the results are interesting for a truly ionogel-based SSE cell operated at ambient temperature with high-energy 4V-class cathode and lithium metal anode (roughly calculating > 400 Wh Kg^{-1} at materials/cell level at C/20 current rate).

Li-metal cell cycling of ionogel composite polymer electrolytes

To combine the beneficial properties of organic and inorganic electrolytes as mentioned in previous paragraphs, particularly trying to improve the cycling behavior at higher current regimes, composite systems were fabricated and their electrochemical behavior was demonstrated by galvanostatic cycling of the Li metal electrode in the PYR/EMI-composite-in-situ-polymerized-on-NMC cathode framework at different current regimes of C/40, C/20, C/10, C/5, and C/20, respectively, between 3.0 and 4.3 V at 25 °C. The same *in-situ* method of UV-polymerizing the ionogel precursor on the surface of the NMC-532 electrode was used to obtain a uniform distribution and intimate contact over the cathodes. In order to prevent short circuits caused by ceramic aggregates, the thickness of the composite electrolytes was fixed to approximately 60 µm, which is thicker than ionogel electrolytes (~30 µm) and, thus, required the use of a relatively lower cathode mass loading. Upon increasing the thickness of the electrolytes, the diffusion path for ions becomes extended, potentially impeding their efficient movement between electrodes. This elongated diffusion distance, resulting from the thicker composite electrolytes, might contribute to the decrease in specific capacity values, in particular at elevated current regimes. In Figure 12, the specific capacities and voltage profiles under different C-rates (1C = 0.32 mA) are shown for PYR-composite (A, B) and for EMI-composite (C, D). Initial discharge capacities of 130 mAh g^{-1} and 150 mAh g^{-1} were obtained at a C/40 rate by the laboratory scale Li-metal cells with PYR-composite and EMI-composite, individually. The specific capacity values progressively increased during initial cycling at a low C/40 rate; this is a peculiar feature indicating that the system undergoes an activation process in the initial stages, where slowly an increasing portion of the active materials is activated at the electrochemical reaction due to improved wettability to the active sites by the electrolyte, with facilitated lithium diffusion, and more active sites for lithium-ion storage.

Overall, for all the samples, the polarization is rather limited, which accounts for an efficient redox reaction kinetics, due to the limited internal resistance at the electrode/electrolyte interface as well as the limited cell overpotential contributions. In general, the materials showed good cycling stability, as for the good overlapping of the charge/discharge curves, accounting for a Coulombic efficiency close to 100% after prolonged cycling, which is a convincing indication of the good interfacial contact between the electrodes and the electrolyte separator. As the applied current increased, the cells showed much more stable cycling capacities under C/20 and C/10 rates, along with high Coulombic efficiency, when compared to the cycling performance of ionogel electrolyte-based cells discussed in the previous paragraph. Even when the cells were operated at C/5, they could still exhibit visible capacities of about 25 mAh g^{-1} (slightly higher with the EMI-composite cell). Moreover, the specific capacities almost recovered to the initial values when returning to C/20 after higher rate cycling, which is an indication of the stability of the whole system. The overall improvement of the electrochemical performance by including LLZO in the composite can be attributed to the improvement of the Li conduction pathways, guaranteeing better stability of the electrode–electrolyte interface. Including ceramic particles mitigates the dendrite formation and inhomogeneity of lithium deposition, thus leading to improved performance, as reported in other literature reports (*21*, *67*, *84–87*). Moreover, the very intimate interconnection between the cell components, as evidenced in SEM images (Figure 10), can facilitate ion transport. Interestingly, despite the sightly ionic conductivity with respect to the parent polymeric ionogels systems, the hybrids showed better electrochemical cycling behavior in the lab-scale Li metal cell at higher C-rates, which is clearly ascribed to the introduction of LLZO likely ameliorating the lithium-ion transport properties, as well as the interfacial characteristics or the mechanical performances, which are also key parameters to allow stable and long-term cycling with lithium metal.

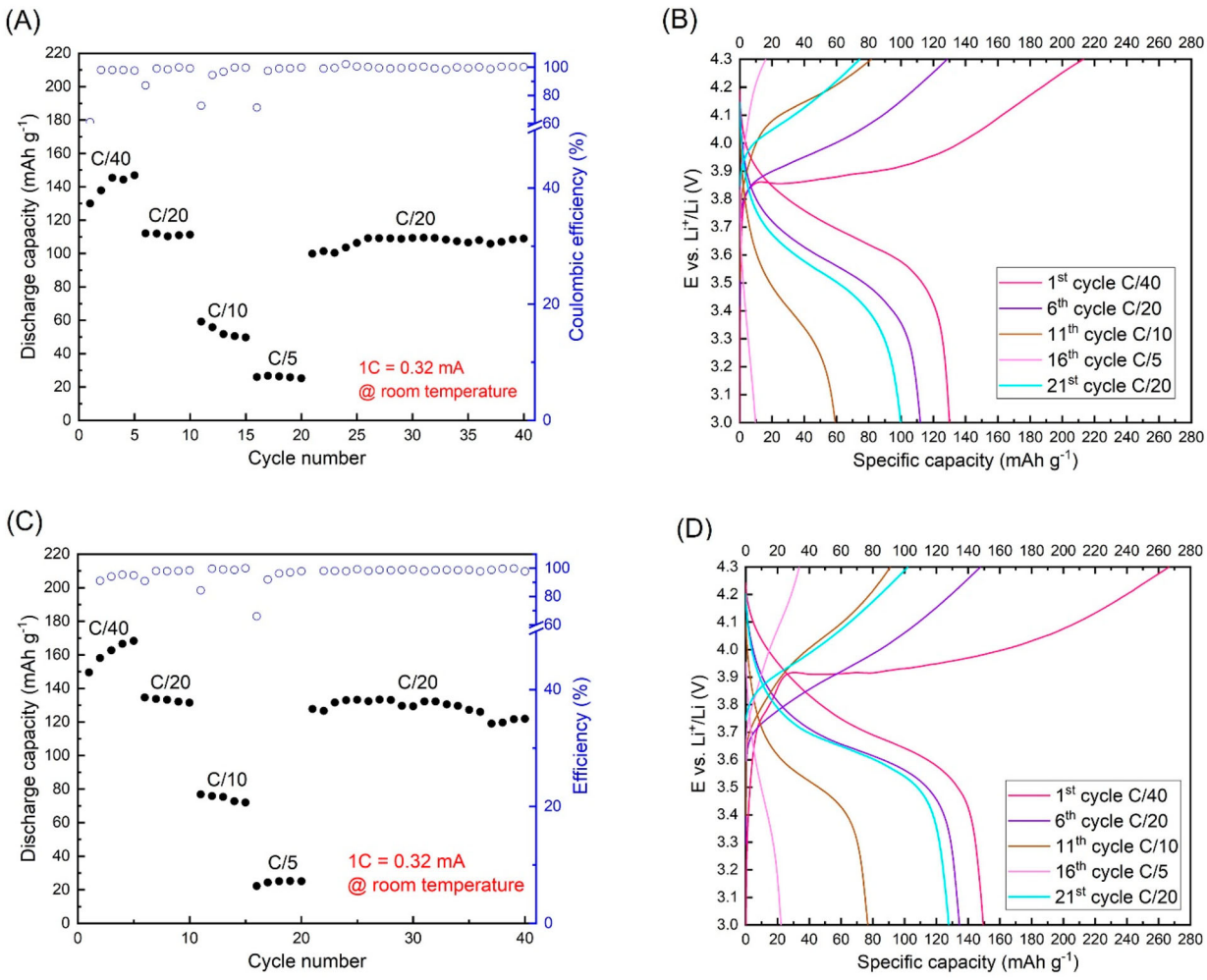

Figure 12. Ambient temperature constant current cycling behavior of the lab-scale cells at different current densities. Specific discharge capacity and Coulombic efficiency vs. cycle number, and discharge/charge potential vs. specific capacity profiles of PYR-composite (A, B) and EMI-composite (C, D).

Conclusion

This work was set out to contribute to the optimization and development of ionogels or hybrid solid polymer electrolytes by understanding the effect of polymer behavior on designing polymer-based solid-state electrolytes (SSEs) with desirable properties. We restricted the choice of chemicals to commercially available components and fabricated two types of ionogel SSEs as well as two types of composite SSEs by introducing LLZO ceramic filler into the ionogel precursors for polymerization. The *in-situ* free-radical polymerization was used to achieve compatible crosslinked solid electrolyte samples during this study. The method was proven to be efficient, controllable, and environmentally friendly. The ionogel formulations resulted in C=C conversions up to 98%, depending on the IL type and the concentration of PI. The imidazolium-IL-containing ionogel exhibited a higher degree of double bond conversion and gel content, which was believed to enhance the cycling performance in a cell with NMC cathodes. The higher viscosity of pyrrolidinium-containing electrolyte samples also affected their polymerization rates and the uniformity of formed matrix structures. Furthermore, the incorporation of LLZO inorganic filler improved the stability of galvanostatic cycling in cells from C/20 to C/5 at room temperature compared to cycling with ionogels. The more porous structure in composites might provide a more favorable ion transport path, and the decreased or trapped unreacted monomer could also contribute to the observed improvement. The proposed methodology represents a promising practical approach for the incorporation of super ion conductors in lithium metal batteries, thus imparting flexibility and shape retention attributes to the separator electrolytes. These findings demonstrate the potential usefulness of investigating the physical properties of polymers in designing

ionogels. Further research could be conducted to elucidate the interaction between the polymer matrix and IL, as well as other ionic compounds in ceramic-rich composite SSEs. This could involve studying molecular engineering aspects of both organic and organic–inorganic ionogels to optimize their performance.

Acknowledgements

This work was supported by the European Union's Horizon 2020 research and innovation program under the Marie Skłodowska-Curie grant agreement No 860403 (European Training Network POLYSTORAGE https://www.polystorage-etn.eu/). Y.Z. would like to acknowledge Dr. Marisa Falco (DISAT, Politecnico di Torino) for the suggestions/opinions on materials preparation, as well as Ms. Sofia Saffirio (DISAT, Politecnico di Torino) for the help with FESEM measurements. This study was carried out within the MOST – Sustainable Mobility Center and received funding from the European Union NextGenerationEU (PIANO NAZIONALE DI RIPRESA E RESILIENZA – PNRR e MISSIONE 4 COMPONENTE 2, INVESTIMENTO 1.4 e D.D. 1033 17/06/2022, CN00000023). This manuscript reflects only the authors' views and opinions, neither the European Union nor the European Commission can be considered responsible for them. Part of this work was carried out within the activities 'Ricerca Sistema Elettrico' funded through contributions to research and development by the Italian Ministry of Economic Development.

Disclosure statement

No potential conflict of interest was reported by the author(s).

Funding

This work was supported by the European Union's Horizon 2020 Research and Innovation framework programme [grant number: 860403].

ORCID

Giuseppe Antonio Elia http://orcid.org/0000-0001-6790-1143
Claudio Gerbaldi http://orcid.org/0000-0002-8084-0143

References

[1] Østergaard, P.A.; Duic, N.; Noorollahi, Y.; Mikulcic, H.; Kalogirou, S. Sustainable Development Using Renewable Energy Technology. *Renew. Energy* **2020**, *146*, 2430–2437. doi: 10.1016/j.renene.2019.08.094.

[2] Abbas, Q.; Mirzaeian, M.; Hunt, M.R.C.; Hall, P.; Raza, R. Current State and Future Prospects for Electrochemical Energy Storage and Conversion Systems. *Energies* **2020**, *13* (21). doi: 10.3390/en13215847.

[3] Ediger, VŞ. An Integrated Review and Analysis of Multi-Energy Transition from Fossil Fuels to Renewables. *Energy Procedia* **2019,** *156*, 2–6. doi: 10.1016/j.egypro.2018.11.073.

[4] Manthiram, A. An Outlook on Lithium Ion Battery Technology. *ACS. Cent. Sci.* **2017,** *3* (10), 1063–1069. doi: 10.1021/acscentsci.7b00288.

[5] Diouf, B.; Pode, R. Potential of Lithium-ion Batteries in Renewable Energy. *Renew. Energy* **2015,** *76*, 375–380. doi: 10.1016/j.renene.2014.11.058.

[6] Kim, T.; Song, W.; Son, D.-Y.; Ono, L.K.; Qi, Y. Lithium-ion Batteries: Outlook on Present, Future, and Hybridized Technologies. *J. Mater. Chem. A* **2019**, *7* (7), 2942–2964. doi: 10.1039/c8ta10513h.

[7] Xu, L.; Tang, S.; Cheng, Y.; Wang, K.; Liang, J.; Liu, C.; Cao, Y.-C.; Wei, F.; Mai, L. Interfaces in Solid-State Lithium Batteries. *Joule* **2018,** *2* (10), 1991–2015. doi: 10.1016/j.joule.2018.07.009.

[8] Chawla, N.; Bharti, N.; Singh, S. Recent Advances in Non-Flammable Electrolytes for Safer Lithium-Ion Batteries. *Batteries* **2019**, *5* (1). doi: 10.3390/batteries5010019.

[9] Xu, K. Nonaqueous Liquid Electrolytes for Lithium-Based Rechargeable Batteries. *Chem. Rev.* **2004**, *104* (10), 4303–4417. doi: 10.1021/cr030203g.

[10] Meutzner F.; de Vivanco, M.U. Electrolytes - Technology review. *AIP Conf. Proc.* **2014,** *1957*, 185–195. doi:10.1063/1.4878487.

[11] Chen, Y.; Kang, Y.; Zhao, Y.; Wang, L.; Liu, J.; Li, Y.; Liang, Z.; He, X.; Li, X.; Tavajohi, N.; Li, B. A Review of Lithium-ion Battery Safety Concerns: The Issues, Strategies, and Testing Standards. *J. Energy Chem.* **2019,** *156*, 83–99. doi: 10.1016/j.jechem.2020.10.017.

[12] Chae, W.; Kim, B.; Ryoo, W.S.; Earmme, T. A Brief Review of Gel Polymer Electrolytes Using In Situ Polymerization for Lithium-ion Polymer Batteries. *Polymers (Basel)* **2023**, *15* (4). doi: 10.3390/polym15040803.

[13] Zhou, D.; Shanmukaraj, D.; Tkacheva, A.; Armand, M.; Wang, G. Polymer Electrolytes for Lithium-Based Batteries: Advances and Prospects. *Chem* **2019,** *5* (9), 2326–2352. doi: 10.1016/j.chempr.2019.05.009.

[14] Schnell, J.; Günther, T.; Knoche, T.; Vieider, C.; Köhler, L.; Just, A.; Keller, M.; Passerini, S.; Reinhart, G. All-solid-state Lithium-ion and Lithium Metal Batteries – Paving the way to Large-Scale Production. *J. Power Sources* **2018,** *382*, 160–175. doi: 10.1016/j.jpowsour.2018.02.062.

[15] Janek, J.; Zeier, W.G. A Solid Future for Battery Development. *Nat. Energy* **2016**, *1* (9). doi: 10.1038/nenergy.2016.141.

[16] Zhao, Q.; Stalin, S.; Zhao, C.-Z.; Archer, L.A. Designing Solid-State Electrolytes for Safe, Energy-Dense Batteries. *Nat. Rev. Mater.* **2020,** *5* (3), 229–252. doi: 10.1038/s41578-019-0165-5.

[17] Yu, X.; Manthiram, A. A Review of Composite Polymer-Ceramic Electrolytes for Lithium Batteries. *Energy Storage Mater.* **2021,** *34*, 282–300. doi: 10.1016/j.ensm.2020.10.006.

[18] Wang, L.; Li, J.; Lu, G.; Li, W.; Tao, Q.; Shi, C.; Jin, H.; Chen, G.; Wang, S. Fundamentals of Electrolytes for Solid-State Batteries: Challenges and Perspectives. *Front. Mater.* **2020**, *7*. doi: 10.3389/fmats.2020.00111.

[19] Meier, K.; Laino, T.; Curioni, A. Solid-State Electrolytes: Revealing the Mechanisms of Li-Ion Conduction in Tetragonal and Cubic LLZO by First-Principles Calculations. *J. Phys. Chem. C* **2014,** *118* (13), 6668–6679. doi: 10.1021/jp5002463.

[20] Wagner, R.; Redhammer, G.J.; Rettenwander, D.; Senyshyn, A.; Schmidt, W.; Wilkening, M.; Amthauer, G. Crystal Structure of Garnet-Related Li-Ion Conductor $Li_{7-3x}Ga_xLa_3Zr_2O_{12}$: Fast Li-Ion Conduction Caused by a Different Cubic Modification? *Chem. Mater.* **2016,** *28* (6), 1861–1871. doi: 10.1021/acs.chemmater.6b00038.

[21] Wang, C.; Fu, K.; Kammampata, S.P.; McOwen, D.W.; Samson, A.J.; Zhang, L.; Hitz, G.T.; Nolan, A.M.; Wachsman, E.D.; Mo, Y.; Thangadurai, V.; Hu, L. Garnet-Type Solid-State Electrolytes: Materials, Interfaces, and Batteries. *Chem. Rev.* **2020,** *120* (10), 4257–4300. doi: 10.1021/acs.chemrev.9b00427.

[22] Verduzco, J.C.; Vergados, J.N.; Strachan, A.; Marinero, E.E. Hybrid Polymer-Garnet Materials for All-Solid-State Energy Storage Devices. *ACS Omega* **2021,** *6* (24), 15551–15558. doi: 10.1021/acsomega.1c01368.

[23] Subramanian, K.; Alexander, G.V.; Karthik, K.; Patra, S.; Indu, M.S.; Sreejith, O.V.; Viswanathan, R.; Narayanasamy, J.; Murugan, R. A Brief Review of Recent Advances in Garnet Structured Solid Electrolyte Based Lithium Metal Batteries. *J. Energy Storage* **2021**, *33*. doi: 10.1016/j.est.2020.102157.

[24] Shiiba, H.; Zettsu, N.; Yamashita, M.; Onodera, H.; Jalem, R.; Nakayama, M.; Teshima, K. Molecular Dynamics Studies on the Lithium Ion Conduction Behaviors Depending on Tilted Grain Boundaries with Various Symmetries in Garnet-Type $Li_7La_3Zr_2O_{12}$. *J. Phys. Chem. C* **2018,** *122* (38), 21755–21762. doi: 10.1021/acs.jpcc.8b06275.

[25] Karasulu, B.; Emge, S.P.; Groh, M.F.; Grey, C.P.; Morris, A.J. Al/Ga-Doped $Li_7La_3Zr_2O_{12}$ Garnets as Li-Ion Solid-State Battery Electrolytes: Atomistic Insights Into Local Coordination Environments and Their Influence on ^{17}O, ^{27}Al, and ^{71}Ga NMR Spectra. *J. Am. Chem. Soc.* **2020,** *142* (6), 3132–3148. doi: 10.1021/jacs.9b12685.

[26] Isaac, J.A.; Devaux, D.; Bouchet, R. Dense Inorganic Electrolyte Particles as a Lever to Promote Composite Electrolyte Conductivity. *Nat. Mater.* **2022,** *21* (12), 1412–1418. doi: 10.1038/s41563-022-01343-w.

[27] Park, M.; Zhang, X.; Chung, M.; Less, G.B.; Sastry, A.M. A Review of Conduction Phenomena in Li-ion Batteries. *J. Power Sources* **2010,** *195* (24), 7904–7929. doi: 10.1016/j.jpowsour.2010.06.060.

[28] Li, S.; Zhang, S.Q.; Shen, L.; Liu, Q.; Ma, J.B.; Lv, W.; He, Y.B.; Yang, Q.H. Progress and Perspective of Ceramic/Polymer Composite Solid Electrolytes for Lithium Batteries. *Adv. Sci.* **2020**, *7* (5). doi: 10.1002/advs.201903088.

[29] Wu, X.; Zheng, Y.; Li, W.; Liu, Y.; Zhang, Y.; Li, Y.; Li, C. Solid Electrolytes Reinforced by Infinite Coordination Polymer Nano-Network for Dendrite-Free Lithium Metal Batteries. *Energy Storage Mater.* **2021,** *41*, 436–447. doi: 10.1016/j.ensm.2021.06.009.

[30] Hu, J.; Chen, K.; Yao, Z.; Li, C. Unlocking Solid-State Conversion Batteries Reinforced by Hierarchical Microsphere Stacked Polymer Electrolyte. *Sci Bull (Beijing)* **2021**, *66* (7), 694–707. doi: 10.1016/j.scib.2020.11.017.

[31] Shin, J. Ionic Liquids to the Rescue? Overcoming the Ionic Conductivity Limitations of Polymer Electrolytes. *Electrochem. Commun.* **2003,** *5* (12), 1016–1020. doi: 10.1016/j.elecom.2003.09.017.

[32] Hu, Y.; Yu, L.; Meng, T.; Zhou, S.; Sui, X.; Hu, X. Hybrid Ionogel Electrolytes for Advanced Lithium Secondary Batteries: Developments and Challenges. *Chem. Asian J.* **2022,** *17* (23), e202200794. doi: 10.1002/asia.202200794.

[33] Galiński, M.; Lewandowski, A.; Stępniak, I. Ionic Liquids as Electrolytes. *Electrochim. Acta* **2006,** *51* (26), 5567–5580. doi: 10.1016/j.electacta.2006.03.016.

[34] Andrzejewska, E. Photoinitiated Polymerization in Ionic Liquids and its Application. *Polym. Int.* **2017,** *66* (3), 366–381. doi: 10.1002/pi.5255.

[35] Ueki, T.; Watanabe, M. Polymers in Ionic Liquids: Dawn of Neoteric Solvents and Innovative Materials. *Bull. Chem. Soc. Jpn.* **2012,** *85* (1), 33–50. doi: 10.1246/bcsj.20110225.

[36] Lewandowski, A.; Świderska-Mocek, A. Ionic Liquids as Electrolytes for Li-ion Batteries - An Overview of Electrochemical Studies. *J. Power Sources* **2009,** *194* (2), 601–609. doi: 10.1016/j.jpowsour.2009.06.089.

[37] Tang, X.; Lv, S.; Jiang, K.; Zhou, G.; Liu, X. Recent Development of Ionic Liquid-Based Electrolytes in Lithium-ion Batteries. *J. Power Sources* **2022**, *542*. doi: 10.1016/j.jpowsour.2022.231792.

[38] Andrzejewska, E.; Marcinkowska, A.; Zgrzeba, A. Ionogels – Materials Containing Immobilized Ionic Liquids. *Polimery* **2017,** *62* (05), 344–352. doi: 10.14314/polimery.2017.344.

[39] Manasa, C.; Basavanna, V.; Ningaiah, S. Ionic Liquid-Based Hybrid Materials: Ionogel Review. *Biointerface Res. Appl. Chem.* **2022**, *13* (4). doi: 10.33263/briac134.391.

[40] Wang, S.; Jiang, Y.; Hu, X. Ionogel-Based Membranes for Safe Lithium/Sodium Batteries. *Adv. Mater.* **2022,** *34* (52), e2200945. doi: 10.1002/adma.202200945.

[41] Park, M.J.; Choi, I.; Hong, J.; Kim, O. Polymer Electrolytes Integrated with Ionic Liquids for Future Electrochemical Devices. *J. Appl. Polym. Sci.* **2013,** *129* (5), 2363–2376. doi: 10.1002/app.39064.

[42] Osada, I.; de Vries, H.; Scrosati, B.; Passerini, S. Ionic-Liquid-Based Polymer Electrolytes for Battery Applications. *Angew. Chem. Int. Ed. Engl.* **2016,** *55* (2), 500–513. doi: 10.1002/anie.201504971.

[43] Sivakkumar, S.R.; MacFarlane, D.R.; Forsyth, M.; Kim, D.-W. Ionic Liquid-Based Rechargeable Lithium Metal-Polymer Cells Assembled with Polyaniline/Carbon Nanotube Composite Cathode. *J. Electrochem. Soc.* **2007,** *154* (9), 6. doi: 10.1149/1.2750443.

[44] Sun, J.; MacFarlane, D.R.; Forsyth, M. Lithium Polyelectrolyte–Ionic Liquid Systems. *Solid State Ionics* **2002,** *147* (3-4), 333–339. doi: 10.1016/S0167-2738(02)00028-0.

[45] Nair, J.R.; Gerbaldi, C.; Meligrana, G.; Bongiovanni, R.; Bodoardo, S.; Penazzi, N.; Reale, P.; Gentili, V. UV-cured Methacrylic Membranes as Novel Gel–Polymer Electrolyte for Li-ion Batteries. *J. Power Sources* **2007,** *178* (2), 751–757. doi: 10.1016/j.jpowsour.2007.08.004.

[46] Porthault, H.; Piana, G.; Cesbron, M.; Armel, V.; Bazin, A.; Franger, S.; Oukassi, S. Photo-Initiated Cross-Linking of a Methacrylate/Ionic Liquid Based Gel Polymer Electrolyte: Effect of the Curing Sequence on the Electrochemical Properties. *J. Phys. Chem. C* **2019,** *123* (30), 18171–18179. doi: 10.1021/acs.jpcc.9b02831.

[47] Susan, M.A.B.H.; Kaneko, T.; Noda, A.; Watanabe, M. Ion Gels Prepared by in Situ Radical Polymerization of Vinyl Monomers in an Ionic Liquid and Their Characterization as Polymer Electrolytes. *J. Am. Chem. Soc.* **2005,** *127* (13), 4976–4983. doi: 10.1021/ja045155b.

[48] Kubisa, P. Kinetics of Radical Polymerization in Ionic Liquids. *Eur. Polym. J.* **2020**, *133*. doi: 10.1016/j.eurpolymj.2020.109778.
[49] Nair, J.R.; Gerbaldi, C.; Destro, M.; Bongiovanni, R.; Penazzi, N. Methacrylic-based Solid Polymer Electrolyte Membranes for Lithium-Based Batteries by a Rapid UV-Curing Process. *React. Funct. Polym.* **2011,** *71* (4), 409–416. doi: 10.1016/j.reactfunctpolym.2010.12.007.
[50] Gerbaldi, C. All-solid-state Lithium-Based Polymer Cells for High-Temperature Applications. *Ionics* **2010,** *16* (9), 777–786. doi: 10.1007/s11581-010-0484-4.
[51] Nair, J.R.; Colò, F.; Kazzazi, A.; Moreno, M.; Bresser, D.; Lin, R.; Bella, F.; Meligrana, G.; Fantini, S.; Simonetti, E.; Appetecchi, G.B.; Passerini, S.; Gerbaldi, C. Room Temperature Ionic Liquid (RTIL)-Based Electrolyte Cocktails for Safe, High Working Potential Li-Based Polymer Batteries. *J. Power Sources* **2019,** *412*, 398–407. doi: 10.1016/j.jpowsour.2018.11.061.
[52] Gerbaldi, C.; Nair, J.R.; Ahmad, S.; Meligrana, G.; Bongiovanni, R.; Bodoardo, S.; Penazzi, N. UV-cured Polymer Electrolytes Encompassing Hydrophobic Room Temperature Ionic Liquid for Lithium Batteries. *J. Power Sources* **2010,** *195* (6), 1706–1713. doi: 10.1016/j.jpowsour.2009.09.047.
[53] Gerbaldi, C.; Nair, J.R.; Meligrana, G.; Bongiovanni, R.; Bodoardo, S.; Penazzi, N. Highly Ionic Conducting Methacrylic-Based Gel-Polymer Electrolytes by UV-Curing Technique. *J. Appl. Electrochem.* **2009,** *39* (11), 2199–2207. doi: 10.1007/s10800-009-9805-6.
[54] Gerbaldi, C.; Nair, J.R.; Ferrari, S.; Chiappone, A.; Meligrana, G.; Zanarini, S.; Mustarelli, P.; Penazzi, N.; Bongiovanni, R. New Electrolyte Membranes for Li-Based Cells: Methacrylic Polymers Encompassing Pyrrolidinium-Based Ionic Liquid by Single Step Photo-Polymerisation. *J. Membr. Sci.* **2012,** *423-424*, 459–467. doi: 10.1016/j.memsci.2012.08.057.
[55] Wang, W.; Alexandridis, P. Composite Polymer Electrolytes: Nanoparticles Affect Structure and Properties. *Polymers (Basel)* **2016**, *8* (11). doi: 10.3390/polym8110387.
[56] Choi, Y.G.; Shin, J.C.; Park, A.; Jeon, Y.M.; Kim, J.I.; Kim, S.; Kim, S.; Lee, W.B.; Lee, M.; Park, J.H. Pyrrolidinium-PEG Ionic Copolyester: Li-Ion Accelerator in Polymer Network Solid-State Electrolytes. *Adv. Energy. Mater.* **2021**, *11* (44). doi: 10.1002/aenm.202102660.
[57] Kerner, M.; Johansson, P. Pyrrolidinium FSI and TFSI-Based Polymerized Ionic Liquids as Electrolytes for High-Temperature Lithium-Ion Batteries. *Batteries* **2018**, *4* (1). doi: 10.3390/batteries4010010.
[58] Lahiri, A.; Schubert, T.J.; Iliev, B.; Endres, F. LiTFSI in 1-Butyl-1-Methylpyrrolidinium bis(Fluorosulfonyl)Amide: A Possible Electrolyte for Ionic Liquid Based Lithium ion Batteries. *Phys. Chem. Chem. Phys.* **2015,** *17* (17), 11161–11164. doi: 10.1039/c5cp01337b.
[59] Kerner, M.; Plylahan, N.; Scheers, J.; Johansson, P. Ionic Liquid Based Lithium Battery Electrolytes: Fundamental Benefits of Utilising Both TFSI and FSI Anions? *Phys. Chem. Chem. Phys.* **2015,** *17* (29), 19569–19581. doi: 10.1039/c5cp01891a.
[60] Corsaro, C.; Neri, G.; Santoro, A.; Fazio, E. Acrylate and Methacrylate Polymers' Applications: Second Life with Inexpensive and Sustainable Recycling Approaches. *Materials (Basel)* **2021**, *15* (1). doi: 10.3390/ma15010282.
[61] Pirman, T.; Ocepek, M.; Likozar, B. Radical Polymerization of Acrylates, Methacrylates, and Styrene: Biobased Approaches, Mechanism, Kinetics, Secondary Reactions, and Modeling. *Ind. Eng. Chem. Res.* **2021,** *60* (26), 9347–9367. doi: 10.1021/acs.iecr.1c01649.
[62] Safranski, D.L.; Gall, K. Effect of Chemical Structure and Crosslinking Density on the Thermo-Mechanical Properties and Toughness of (Meth)Acrylate Shape Memory Polymer Networks. *Polymer* **2008,** *49* (20), 4446–4455. doi: 10.1016/j.polymer.2008.07.060.
[63] Noe, C.; Tonda-Turo, C.; Chiappone, A.; Sangermano, M.; Hakkarainen, M. Light Processable Starch Hydrogels. *Polymers (Basel)* **2020**, *12* (6). doi: 10.3390/polym12061359.
[64] Endruweit, A.; Johnson, M.S.; Long, A.C. Curing of Composite Components by Ultraviolet Radiation: A Review. *Polym. Compos.* **2006,** *27* (2), 119–128. doi: 10.1002/pc.20166.
[65] Zagórski, J.; Silván, B.; Saurel, D.; Aguesse, F.; Llordés, A. Importance of Composite Electrolyte Processing to Improve the Kinetics and Energy Density of Li Metal Solid-State Batteries. *ACS Appl. Energy Mater.* **2020,** *3* (9), 8344–8355. doi: 10.1021/acsaem.0c00935.
[66] Nguyen, Q.H.; Luu, V.T.; Nguyen, H.L.; Lee, Y.W.; Cho, Y.; Kim, S.Y.; Jun, Y.S.; Ahn, W. $Li_7La_3Zr_2O_{12}$ Garnet Solid Polymer Electrolyte for Highly Stable All-Solid-State Batteries. *Front. Chem.* **2020,** *8*, 619832. doi: 10.3389/fchem.2020.619832.
[67] Luu, V.T.; Nguyen, Q.H.; Park, M.G.; Nguyen, H.L.; Seo, M.-H.; Jeong, S.-K.; Cho, N.; Lee, Y.-W.; Cho, Y.; Lim, S.N.; Jun, Y.-S.; Ahn, W. Cubic Garnet Solid Polymer Electrolyte for Room Temperature Operable All-Solid-State-Battery. *J. Mater. Res. Technol.* **2021**. doi: 10.1016/j.jmrt.2021.11.055.
[68] Dirican, M.; Yan, C.; Zhu, P.; Zhang, X. Composite Solid Electrolytes for All-Solid-State Lithium Batteries. *Mater. Sci. Eng. R Rep.* **2019,** *136*, 27–46. doi: 10.1016/j.mser.2018.10.004.
[69] Kravchyk, K.V.; Karabay, D.T.; Kovalenko, M.V. On the Feasibility of All-Solid-State Batteries with LLZO as a Single Electrolyte. *Sci. Rep.* **2022,** *12* (1), 1177. doi: 10.1038/s41598-022-05141-x.
[70] Falco, M.; Castro, L.; Nair, J.R.; Bella, F.; Bardé, F.; Meligrana, G.; Gerbaldi, C. UV-Cross-Linked Composite Polymer Electrolyte for High-Rate, Ambient Temperature Lithium Batteries. *ACS Appl. Energy Mater.* **2019,** *2* (3), 1600–1607. doi: 10.1021/acsaem.8b02185.
[71] Noè, C.; Hakkarainen, M.; Malburet, S.; Graillot, A.; Adekunle, K.; Skrifvars, M.; Sangermano, M. Frontal-Photopolymerization of Fully Biobased Epoxy Composites. *Macromol. Mater. Eng.* **2022**, *307* (6). doi: 10.1002/mame.202100864.
[72] Tkachenko, Y.; Niedzielski, P. FTIR as a Method for Qualitative Assessment of Solid Samples in Geochemical Research: A Review. *Molecules* **2022**, *27* (24). doi: 10.3390/molecules27248846.
[73] Agafonov, A.V.; Grishina, E.P.; Kudryakova, N.O.; Ramenskaya, L.M.; Kraev, A.S.; Shibaeva, V.D. Ionogels: Squeeze Flow Rheology and Ionic Conductivity of Quasi-Solidified Nanostructured Hybrid Materials Containing Ionic Liquids Immobilized on Halloysite. *Arab. J. Chem.* **2022**, *15* (1). doi: 10.1016/j.arabjc.2021.103470.

[74] Liew, C.W.; Durairaj, R.; Ramesh, S. Rheological Studies of PMMA-PVC Based Polymer Blend Electrolytes with LiTFSI as Doping Salt. *PLoS One* **2014,** *9* (7), e102815. doi: 10.1371/journal.pone.0102815.

[75] Doumeng, M.; Berthet, F.; Delbé, K.; Marsan, O.; Denape, J.; Chabert, F. Effect of Size, Concentration, and Nature of Fillers on Crystallinity, Thermal, and Mechanical Properties of Polyetheretherketone Composites. *J. Appl. Polym. Sci.* **2021**, *139* (5). doi: 10.1002/app.51574.

[76] Liang, W.; Shao, Y.; Chen, Y.-M.; Zhu, Y. A 4V Cathode Compatible, Superionic Conductive Solid Polymer Electrolyte for Solid Lithium Metal Batteries with Long Cycle Life. *ACS Appl. Energy Mater.* **2018,** *1* (11), 6064–6071. doi: 10.1021/acsaem.8b01138.

[77] Xu, X.; Lee, S.; Jeong, S.; Kim, Y.; Cho, J. Recent Progress on Nanostructured 4 V Cathode Materials for Li-ion Batteries for Mobile Electronics. *Mater. Today* **2013,** *16* (12), 487–495. doi: 10.1016/j.mattod.2013.11.021.

[78] Porcarelli, L.; Gerbaldi, C.; Bella, F.; Nair, J.R. Super Soft All-Ethylene Oxide Polymer Electrolyte for Safe All-Solid Lithium Batteries. *Sci. Rep.* **2016,** *6*, 19892. doi: 10.1038/srep19892.

[79] Chiappone, A.; Nair, J.R.; Gerbaldi, C.; Bongiovanni, R.; Zeno, E. UV-cured Al_2O_3-Laden Cellulose Reinforced Polymer Electrolyte Membranes for Li-Based Batteries. *Electrochim. Acta* **2015,** *153*, 97–105. doi: 10.1016/j.electacta.2014.11.141.

[80] Nair, J.R.; Destro, M.; Gerbaldi, C.; Bongiovanni, R.; Penazzi, N. Novel Multiphase Electrode/Electrolyte Composites for Next Generation of Flexible Polymeric Li-ion Cells. *J. Appl. Electrochem.* **2012,** *43* (2), 137–145. doi: 10.1007/s10800-012-0492-3.

[81] Zhao, Q.; Liu, X.; Stalin, S.; Khan, K.; Archer, L.A. Solid-state Polymer Electrolytes with in-Built Fast Interfacial Transport for Secondary Lithium Batteries. *Nat. Energy* **2019,** *4* (5), 365–373. doi: 10.1038/s41560-019-0349-7.

[82] Vijayakumar, V.; Anothumakkool, B.; Kurungot, S.; Winter, M.; Nair, J.R. In Situ Polymerization Process: An Essential Design Tool for Lithium Polymer Batteries. *Energy Environ. Sci.* **2021,** *14* (5), 2708–2788. doi: 10.1039/d0ee03527k.

[83] Liao, C.; Sun, X.-G.; Dai, S. Crosslinked gel Polymer Electrolytes Based on Polyethylene Glycol Methacrylate and Ionic Liquid for Lithium ion Battery Applications. *Electrochim. Acta* **2013,** *87*, 889–894. doi: 10.1016/j.electacta.2012.10.027.

[84] Tsurumaki, A.; Rettaroli, R.; Mazzapioda, L.; Navarra, M.A. Inorganic–Organic Hybrid Electrolytes Based on Al-Doped $Li_7La_3Zr_2O_{12}$ and Ionic Liquids. *Appl. Sci.* **2022**, *12* (14). doi: 10.3390/app12147318.

[85] Zhang, L.; Zhuang, Q.; Zheng, R.; Wang, Z.; Sun, H.; Arandiyan, H.; Wang, Y.; Liu, Y.; Shao, Z. Recent Advances of $Li_7La_3Zr_2O_{12}$-Based Solid-State Lithium Batteries Towards High Energy Density. *Energy Storage Mater.* **2022,** *49*, 299–338. doi: 10.1016/j.ensm.2022.04.026.

[86] Lechartier, M.; Porcarelli, L.; Zhu, H.; Forsyth, M.; Guéguen, A.; Castro, L.; Mecerreyes, D. Single-ion Polymer/LLZO Hybrid Electrolytes with High Lithium Conductivity. *Mater. Adv.* **2022,** *3* (2), 1139–1151. doi: 10.1039/d1ma00857a.

[87] Li, Z.; Huang, H.M.; Zhu, J.K.; Wu, J.F.; Yang, H.; Wei, L.; Guo, X. Ionic Conduction in Composite Polymer Electrolytes: Case of PEO:Ga-LLZO Composites. *ACS Appl. Mater. Interfaces* **2019,** *11* (1), 784–791. doi: 10.1021/acsami.8b17279.